A&A 618, A4 (2018)
https://doi.org/10.1051/0004-6361/201833335

Astronomy & Astrophysics

IRC +10216 as a spectroscopic laboratory: improved rotational constants for SiC_2, its isotopologues, and Si_2C[⋆,⋆⋆]

J. Cernicharo[1], M. Guélin[2], M. Agúndez[1], J. R. Pardo[1], S. Massalkhi[1], J. P. Fonfría[1], L. Velilla Prieto[1], G. Quintana-Lacaci[1], N. Marcelino[1], C. Marka[3], S. Navarro[3], and C. Kramer[3]

[1] Group of Molecular Astrophysics, Instituto de Física Fundamental, CSIC, C/ Serrano 123, 28006 Madrid, Spain
e-mail: jose.cernicharo@csic.es
[2] Institut de Radioastronomie Millimétrique, 300 rue de la Piscine, 38406 Saint Martin d'Hères, France
[3] Instituto de Radioastronomía Milimétrica, Avenida Divina Pastora 7, 18012 Granada, Spain

Received 1 May 2018 / Accepted 4 June 2018

ABSTRACT

This work presents a detailed analysis of the laboratory and astrophysical spectral data available for $^{28}SiC_2$, $^{29}SiC_2$, $^{30}SiC_2$, $Si^{13}CC$, and Si_2C. New data on the rotational lines of these species between 70 and 350 GHz have been obtained with high spectral resolution (195 kHz) with the IRAM 30 m telescope in the direction of the circumstellar envelope IRC +10216. Frequency measurements can reach an accuracy of 50 kHz for features observed with a good signal to noise ratio. From the observed astrophysical lines and the available laboratory data new rotational and centrifugal distortion constants have been derived for all the isotopologues of SiC_2, allowing us to predict their spectrum with an estimated accuracy better than 50 kHz below 500 GHz and around 50–100 kHz for the strong lines above 500 GHz. Improved rotational and centrifugal distortion constants have also been obtained for disilicon carbide, Si_2C. This work shows that observations of IRC +10216 taken with the IRAM 30 m telescope, with a spectral resolution of 195 kHz, can be used for any molecular species detected in this source to derive, or improve, its rotational constants. Hence, IRC +10216 in addition to be one the richest sources in molecular species in the sky, can also be used as a spectroscopy laboratory in the millimetre and submillimetre domains.

Key words. molecular data – line: identification – stars: carbon – circumstellar matter – stars: individual: IRC +10216 – astrochemistry

1. Introduction

Due to its close proximity (~130 pc), IRC +10216, the circumstellar envelope of CW Leo, has attracted many studies because it is exceptionally rich in molecular species. Half of the known interstellar species are observed in this C-rich envelope. The observed molecules range from CO, the main tracer of the cool molecular gas, and other diatomic and triatomic species (see e.g. Cernicharo et al. 2000, 2010), to molecules containing refractory elements (Cernicharo & Guélin 1987), long carbon chain species C_nH and their anions (Cernicharo & Guélin 1996; Cernicharo et al. 2008; Guélin et al. 1997; McCarthy et al. 2006; Thaddeus et al. 2008, and references therein). Silicon-carbon species such as SiC_2 (Thaddeus et al. 1984), SiC (Cernicharo et al. 1989), SiC_3 (Apponi et al. 1999), SiC_4 (Ohishi et al. 1989), and Si_2C (Cernicharo et al. 2015a) have been also detected in IRC +10216.

Silicon dicarbide, SiC_2, is the most abundant silicon-carbon bearing species in the circumstellar envelopes of carbon-rich evolved stars. These objects show prominent absorption bands in the optical. Although many of these bands can be attributed to C_2 and CN, a series of bands discovered by Merrill (1926) and Sanford (1926) remained unidentified for long time. These bands are typical of N-type stars and have been studied in detail by Sarre et al. (2000). The first indication on the presence of a molecule containing silicon and carbon as responsible of the Merrill–Sanford bands was obtained by Kleman (1956) through the comparison of these absorption bands with laboratory spectra of SiC products obtained by heating silicon to 2500 K in the graphite tube of a King furnace. He concluded that the best candidate was SiC_2, and assumed that the molecule was linear by analogy with C_3. However, ab initio calculations (Grev & Schaefer 1984) and laboratory spectroscopy of jet-cooled SiC_2 (Bondybey 1982; Michalopoulos et al. 1984) indicated that the most stable isomer of SiC_2 has a triangular configuration. Based on these assumptions, and on the rotational constants derived by Michalopoulos et al. (1984), nine previously unidentified features in IRC +10216 were assigned to rotational transitions of SiC_2 (Thaddeus et al. 1984). This identification was supported by the excellent fit of the astronomical frequencies to an asymmetric top with C_{2v} symmetry (lacking rotational levels with odd values for K_a due to the two equivalent C nuclei) and on the reasonable agreement with the rotational constants derived from optical data by Michalopoulos et al. (1984). The identification was fully supported by the detection of the isotopologues $^{29}SiC_2$ and $^{30}SiC_2$ based on astronomical data of IRC +10216 (Cernicharo et al. 1986a). Moreover, a detailed analysis of the electronic bands of SiC_2 observed in the laboratory by Bredohl et al. (1988) allowed measurement of high-J and high-K transitions providing a more precise determination of the rotational

⋆ This work is based on observations carried out with the IRAM 30-m telescope. IRAM is supported by INSU/CNRS (France), MPG (Germany), and IGN (Spain).
⋆⋆ Tables A.2, A.5, A.8, A.11 and A.14 are only available at the CDS via anonymous ftp to cdsarc.u-strasbg.fr (130.79.128.5) or via http://cdsarc.u-strasbg.fr/viz-bin/qcat?J/A+A/618/A4

and centrifugal distortion constants of SiC_2 which were in very good agreement with those derived by Thaddeus et al. (1984).

Millimetre-wave laboratory spectroscopy of SiC_2 was finally carried out by Gottlieb et al. (1989), who measured 41 rotational lines between 93 and 369 GHz. The dipole moment of the molecule was measured by Suenram et al. (1989), who also reported the frequency of the $1_{01} \rightarrow 0_{00}$ transition in the centimetre-wave domain for $^{28}SiC_2$, $^{29}SiC_2$, and $^{30}SiC_2$. Laboratory spectroscopy for $Si^{13}CC$ was performed by Cernicharo et al. (1991). More recently, a significant number of lines have been measured by Kokkin et al. (2011) for $^{29}SiC_2$ and $^{30}SiC_2$. Until these recent measurements, frequency predictions for these two isotopologues were based on the fit to the astronomical lines reported by Cernicharo et al. (1986a, 1991, 2000) and the $1_{01} \rightarrow 0_{00}$ transition measured by Suenram et al. (1989).

Observations of IRC +10216 by Cernicharo et al. (2010) using the HIFI instrument (de Graauw et al. 2010) on board the *Herschel* satellite (Pilbratt et al. 2010) revealed around 300 features between 480 GHz and 1 THz that could be attributed to SiC_2. A detailed study of these lines was carried out by Müller et al. (2012) who provided a global fit to the laboratory and astronomical lines of SiC_2 at that time.

Since its detection in 1984 by Thaddeus et al., SiC_2 has been observed towards the envelopes of carbon-rich stars through its rotational transitions in the millimetre and submillimetre domains. Compared with the Merrill–Sanford band that traces SiC_2 between the photosphere of the star and a few stellar radii, the rotational lines bring information on the whole circumstellar envelope of these objects. SiC_2 is assumed, together with Si_2C (Cernicharo et al. 2015a), to be precursor of SiC dust. Its spatial distribution is only known in IRC +10216 where it was observed with the Plateau de Bure interferometer (Guélin et al. 1993), and the ALMA interferometer (Velilla Prieto et al. 2015). Silicon carbides, and in particular SiC, have been detected only in the external shells (300 R_* and beyond) of IRC +10216 (Cernicharo et al. 1989; Patel et al. 2013). Hence, it seems that it does not contribute to the formation of SiC dust. The presence of SiC grains in C-rich AGBs was confirmed by the detection of an emission band at ~11.3 μm (Hackwell 1972; Treffers & Cohen 1974). This band has been found towards a large number of C-rich stars by the IRAS and ISO satellites (see, e.g. Little-Marenin 1986; Chan & Kwok 1990; Yang et al. 2004). In a recent study using the IRAM 30 m telescope, Massalkhi et al. (2018) have concluded, through the observation of 25 C-rich stars, that the denser the envelope, the less abundant SiC_2. This observed trend has been interpreted as an evidence of efficient incorporation of SiC_2 onto dust grains. A detailed analysis of the rotational excitation of SiC_2 has also been carried out by these authors.

The sensitivity that can be reached with the IRAM 30 m telescope or with ALMA (Cernicharo et al. 2013) allows to detect weak lines of abundant species at well-known frequencies. As an example, the SiC_2 strongest features towards IRC +10216 reach 2–3 K when observed with the IRAM 30 m telescope. The sensitivity of the receivers and backends in this telescope allows to detect, in reasonable integration times, features that are 500–1000 times weaker. When interpreting the densely populated spectrum of this source it is mandatory to identify all these weak features before new molecular species could be assigned. The problem when observing this type of source is that there is a large range of gas temperatures, between 20 and 2500 K, and, hence, many rotational levels are populated in the ground and vibrationally excited states of abundant species (Cernicharo et al. 2013). Frequencies for these transitions are not always very well predicted from the available laboratory work. Consequently, we rely directly upon the astronomical frequencies derived from observations of this kind of objects or of hot cores (Tercero et al. 2010).

This work presents an accurate determination of frequencies for all rotational lines of SiC_2, its isotopologues, and Si_2C, observed with antenna temperatures above a few mK at a spectral resolution of 195 kHz with the IRAM 30 m telescope. It is shown that the frequency determination, despite the broad features exhibited by these rotational transitions, can be as accurate as 50 kHz which competes well with the accuracy obtained in the laboratory in the millimetre and submillimetre domains. A new set of rotational and centrifugal distortion constants has then been obtained for SiC_2, $^{29}SiC_2$, $^{30}SiC_2$, and $Si^{13}CC$ which are recommended to predict the spectrum of these molecules up to 1 THz. For Si_2C the new set of molecular parameters could be used to predict the frequencies up to 500 GHz.

The observations are described in Sect. 2 and the frequency accuracy claimed in this work is justified in Sect. 3. The analysis of the observed rotational lines of these species, and the rotational and centrifugal distortion constants derived from a fit to these lines, are given in Sects. 4.1–4.4.

2. Observations

Our long-term (~30 yr) search for new molecules in IRC +10216 has covered a large fraction of the λ 3, 2, 1 and 0.8 mm bands using the IRAM 30 m radio telescope (see Cernicharo et al. 2015a) reaching a high signal to noise ratio. For frequencies above 280 GHz the spectrometers were two autocorrelators with 2 MHz spectral resolution and 4 GHz bandwidth. For all other observations before 2010 the spectral resolution was 1 MHz provided by filter banks or autocorrelators. The whole data set has been described by Cernicharo et al. (2017). In this paper we focus on data acquired after 2010, when the new Fast Fourier Transform spectrometers, which cover a bandwidth of 2×16 GHz with a spectral resolution of 195 kHz, and the new EMIR receivers which provide an instantaneous bandwidth of 16 GHz, were installed at the 30 m telescope.

The whole λ 2 mm band has been covered in a line survey of IRC +10216 carried out by Cernicharo et al. (2000). New sensitive observations in this band were performed in January and April 2017. The rms of the merged (old and new) 2 mm observations varies between 0.6 and 1.3 mK for a spectral resolution of 1 MHz, and between 2 and 5 mK for a spectral resolution of 195 kHz (new data). The new 3 mm, 1 mm and 0.8 mm data come from observations carried out during the searches quoted by Cernicharo et al. (2017), a time variability monitoring of IRC +10216 started in 2015 (Pardo et al. 2018), and from specific sensitive observations looking for lines of methyl silane in January 2017 (Cernicharo et al. 2017).

The observing mode, in which we wobbled the secondary mirror by ±90″ at a rate of 0.5 Hz, and the dry weather conditions (sky opacity at 225 GHz was below 0.1 most of the observing time) ensured flat baselines and low system noise temperatures ($T_{sys} \simeq$ 100–400 K depending on the frequency). This observing method, with the off position located at 180″ from the star, provides reference data free from emission from all molecular species but CO (see Cernicharo et al. 2015b). The emission of all other molecular species is restricted to a region ≤15–20″ from the star (see, e.g. Guélin et al. 1993; Agúndez et al. 2015, 2017; Velilla Prieto et al. 2015; Quintana-Lacaci et al. 2016). Each frequency setup was observed for ~2 h, with pointing and focus checks in between using strong nearby quasars. Pointing corrections were

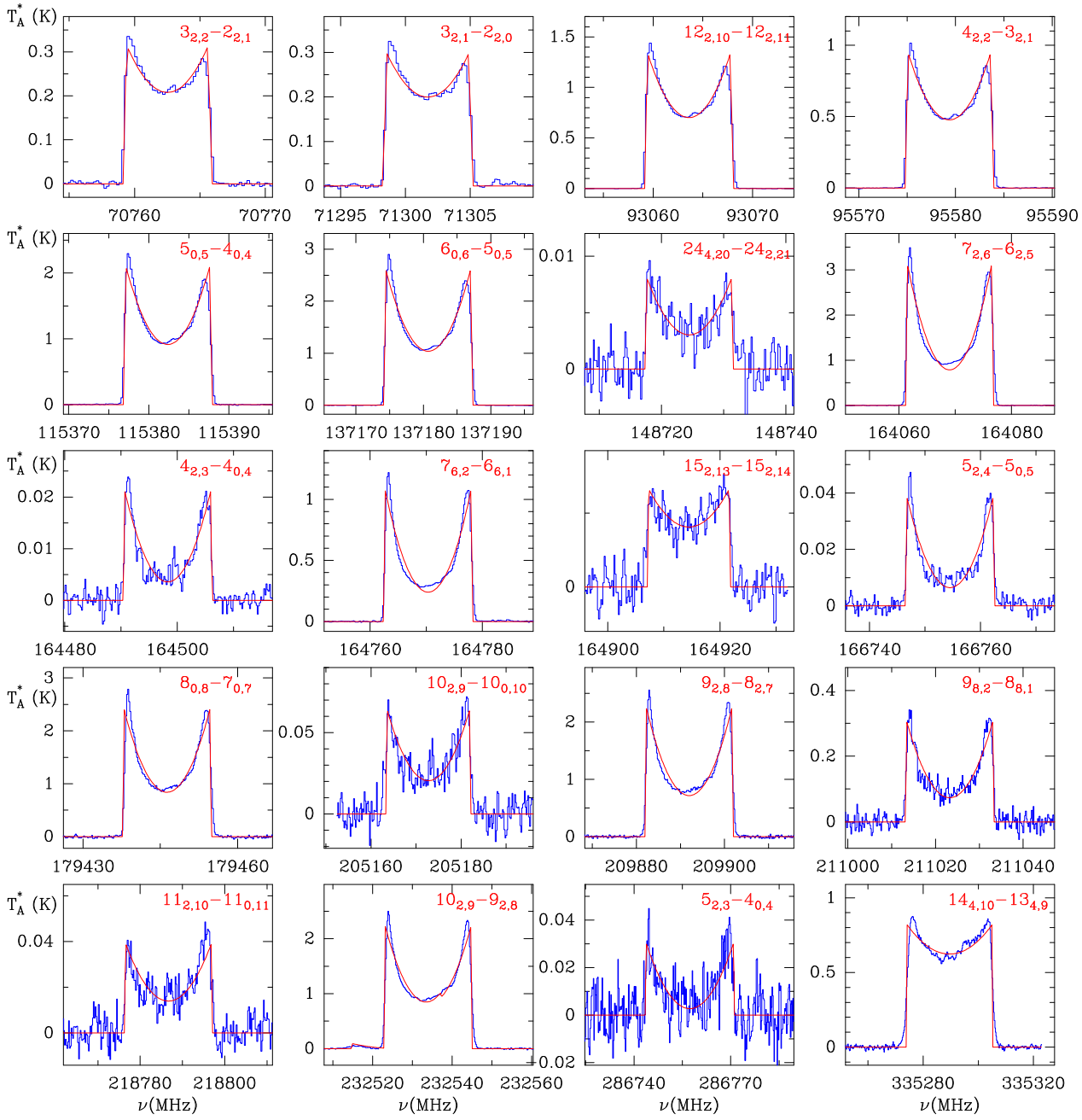

Fig. 1. Selected $^{28}SiC_2$ lines observed in IRC +10216 with the IRAM 30 m telescope with a spectral resolution of 195 kHz. Abscissa is frequency in MHz and the intensity scale is in antenna temperature. The fitted line profile (see Sect. 3) is shown in red. Quantum numbers for the rotational transitions shown in this figure are indicated at the top-right corner of each panel. Measured and fitted rest frequencies are given in Table A.2.

always within 2–3″. The 30 m beam sizes are in the ranges 30″–21″ at 3 mm, 20″–17″ at 2 mm, and 12″–9″ at 1 mm. The intensity scale, antenna temperature (T_A^*), was corrected for atmospheric absorption using the ATM package (Cernicharo 1985; Pardo et al. 2001). Calibration uncertainties for data covering such a large observing period have been adopted to be 10%, 15%, 20%, and 30% at 3, 2, 1, and 0.8 mm, respectively. Additional uncertainties could arise from line intensity fluctuations with time induced by the variation of the stellar infrared flux (Cernicharo et al. 2014; Pardo et al. 2018).

Figure 1 shows selected lines of $^{28}SiC_2$ observed at a spectral resolution of 195 kHz with the new EMIR receivers and FTS spectrometers.

3. Frequency measurements and frequency accuracy using IRC +10216 as a spectroscopic laboratory

All lines of SiC_2 and its isotopologues have been analysed using the CLASS programme from the GILDAS package[1]. This software allows to simultaneously fit several lines in a given spectrum using two different methods. The standard fit, which considers Gaussian line profiles, cannot be used for expanding envelopes. The second method (called *SHELL*) allows fitting the profile of a line emerging from an expanding atmosphere. The

[1] http://www.iram.fr/IRAMFR/GILDAS

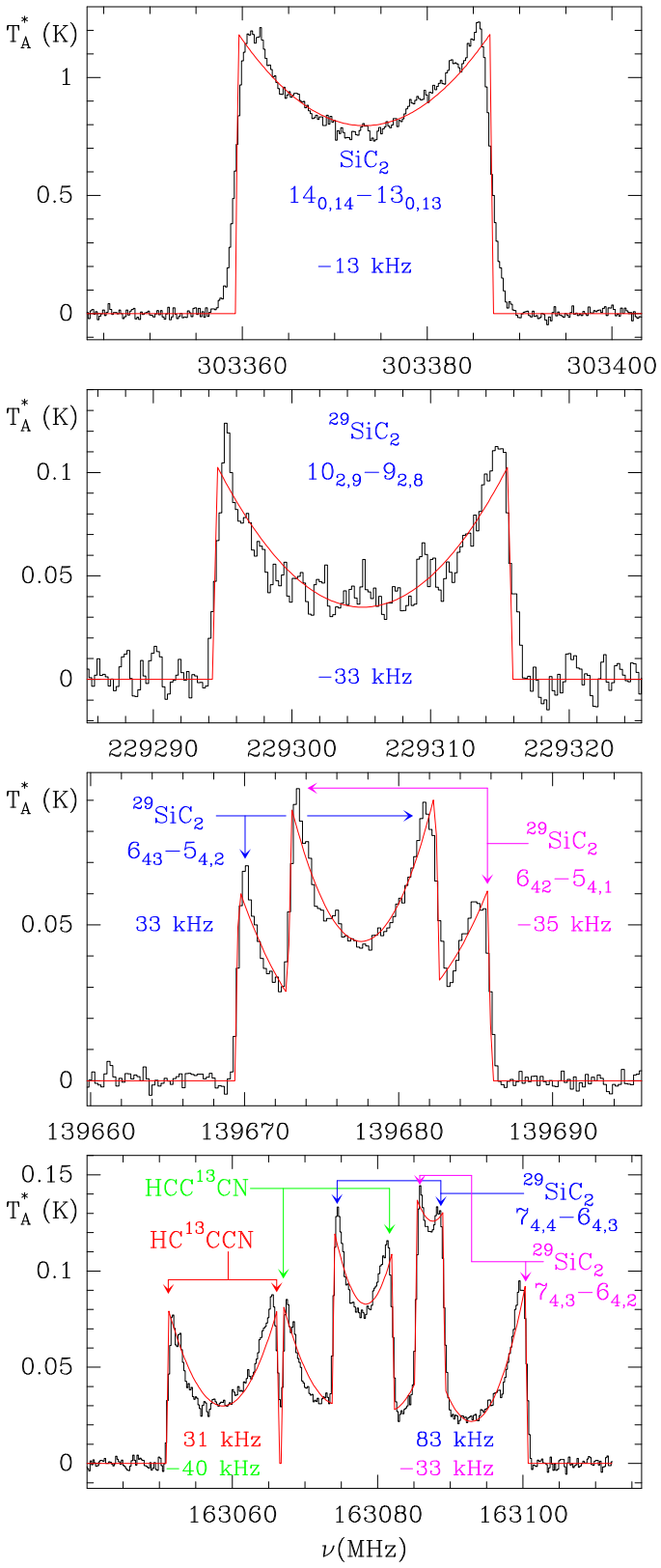

Fig. 2. Some of the lines used in the fit to obtain the rotational constants of SiC_2 and its isotopologues. The fitted line profile is shown in red. Line identification is provided in each panel. Abscissa is frequency in MHz and the intensity scale corresponds to T_A^*. Numbers in each panel indicate the difference between laboratory frequencies (or predicted frequencies from laboratory data) minus the derived frequency of the lines observed towards IRC +10216 using the *SHELL* fitting method (see text).

fitting function is given, on the assumption the line profile is symmetric about line centre, by (see GILDAS documentation[2]):

$$\phi(v) = \frac{A}{\Delta v}\frac{1 + 4H[(v - v_0)/\Delta v]^2}{1 + H/3}. \quad (1)$$

The parameters in Eq. (1) are the integrated intensity A, the centre frequency v_0, the full width at zero level Δv, and the horn to centre intensity ratio H. The shape of the profile varies from a parabola ($H = -1$), as exhibited by optically thick lines, to flat-topped lines ($H = 0$) corresponding to unresolved optically thin lines, and double peaked profiles ($H > 0$) produced by resolved optically thin lines. The expansion velocity of the envelope, v_{exp}, is given by

$$v_{exp} = \frac{c\Delta v}{2v_0}, \quad (2)$$

where c is the speed of light.

The lines in IRC +10216 are broad but most of them are characterized by a U-shape profile with two strong peaks separated from the central frequency by $\pm v_{exp}$. Figure 2 shows some examples of observed and fitted line profiles for the different isotopologues of SiC_2. In previous observations of IRC +10216 (Cernicharo et al. 2000), the spectral resolution of the observations was 1 MHz and the uncertainties on the frequency estimates were, in the case of high signal to noise ratio and symmetric lines, of the order of 0.2–0.3 MHz at most. Present observations have a spectral resolution five times better and, hence, frequency estimates are more precise.

3.1. Error estimates

In order to check the frequency accuracy that could be obtained from the new data, we have compared the laboratory measured frequencies, or frequency predictions using rotational and distortion constants obtained from laboratory data, with those obtained for 255 lines observed in IRC +10216 belonging to different species with a well characterized spectrum in the laboratory (frequency predictions accurate to within a few kHz). Figure 3 shows the differences (hereafter referred as δ_v) between laboratory, or predicted frequencies, and those derived from our astronomical data. Laboratory frequencies for SiC_2 are from Gottlieb et al. (1989), and those for $^{29}SiC_2$ and $^{30}SiC_2$ from Kokkin et al. (2011). For the frequencies of the other species shown in this figure we have adopted the recommended frequencies from the CDMS (Müller et al. 2005), JPL (Pickett et al. 1998), or those calculated by the MADEX[3] code (Cernicharo 2012).

Most of the measured δ_v values are below 50 kHz. The *SHELL* method in GILDAS does not take into account the turbulent velocity of the gas which is easily seen in optically thick lines (see top panel of Fig. 2). Nevertheless, frequencies can still be derived quite accurately as the turbulent velocity affects in the same way the red and blue edges of the line. As an example, for the rotational transition of SiC_2 shown in the top panel of Fig. 2, δ_v is −13 kHz.

For optically thin lines the central frequency is very well constrained by the rather sharp edges of the line profile (see the lines of $^{29}SiC_2$ in the three bottom panels of Fig. 2) and by the two

[2] https://www.iram.fr/IRAMFR/GILDAS/doc/html/class-html/node38.html
[3] http://www.icmm.csic.es/nanocosmos/?page_id=1619

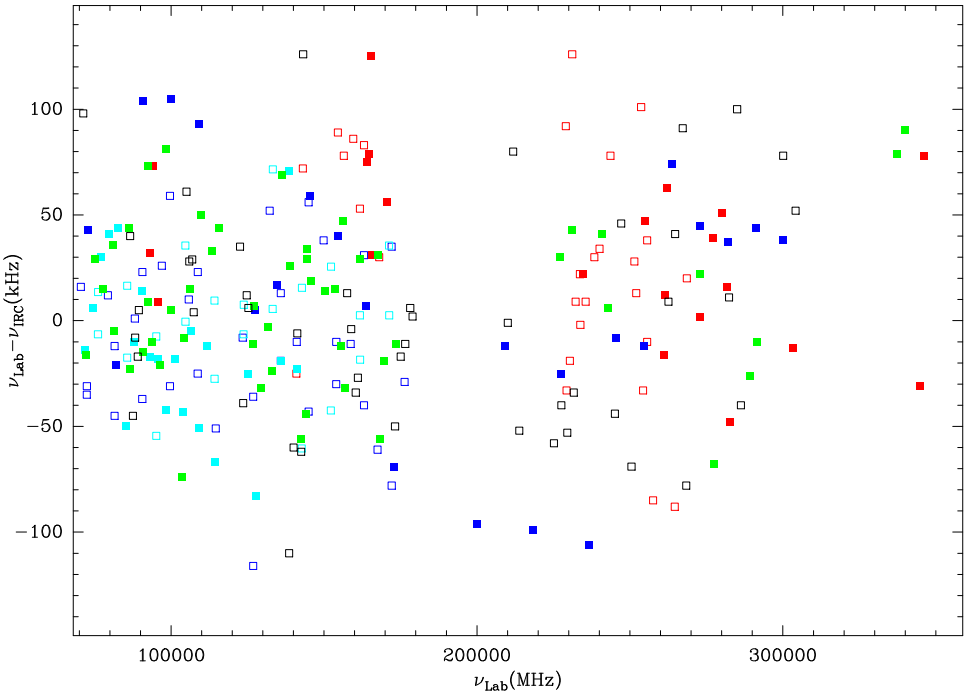

Fig. 3. Laboratory frequencies (or predicted frequencies from laboratory data) minus observed frequencies in IRC +10216 (in kHz) as a function of the frequency of the lines. The different symbols correspond to the following molecules: SiC_2 (red filled squares); $^{29}SiC_2$ and $^{30}SiC_2$ (red empty squares); HC_3N (blue filled squares); the three ^{13}C isotopologues of HC_3N (blue empty squares); HC_5N (cyan filled squares); C_4H (cyan empty squares); ^{13}CS, $C^{34}S$, $C^{33}S$, $^{13}C^{34}S$, CCS, and CCCS (green filled squares); ^{29}SiS, ^{30}SiS, $Si^{34}S$, $Si^{33}S$, and $^{29}Si^{34}S$ (black empty squares).

emission peaks appearing at the terminal expanding velocity of the circumstellar envelope with nearly similar intensities. Even when lines are blended, but the edges of the line are still clearly distinguished, the derived frequencies are in very good agreement with laboratory measurements (see the two bottom panels of Fig. 2).

The fitting procedure assigns very optimistic uncertainties to the fitted frequency, typically a few kHz. Although Fig. 3 shows that frequency determinations in IRC +10216 can be very precise, for the purpose of using the frequencies to derive rotational and centrifugal distortion constants we have considered less optimistic errors. We have systematically assigned a frequency uncertainty of 50 kHz when the CLASS fitting routine provided a frequency uncertainty below 50 kHz, and the nearest multiple of 50 (100, 150, ... kHz) when the fitting algorithm yielded frequency errors >50 kHz. Only a few astronomical lines in Fig. 3 have uncertainties larger than 50 kHz. They are lines heavily blended with other features.

3.2. Systematic effects in estimating line frequencies

Some systematic effects could appear in the derived frequencies for U-shaped lines with different intensities in the blue and red peaks. For C_4H, which presents very different intensities in the two peaks, the measured frequencies from IRC +10216 data are systematically shifted by −50 kHz. This effect results from the fitting algorithm trying to find the best centroid for the line. Such systematic shift in the derived frequencies is also found for the radicals C_3H, C_4H, and C_3N, which exhibit extremely U-shaped line profiles (with the blue component being 20–30% weaker than the red one) and very weak emission around the line centre, that is, a very high horn over centre intensity ratio ($H \gg 0$). Several lines of SiC_2 show asymmetries in the line intensity between the blue and red peaks of the line profile (see Fig. 1). However, the emission around the line centre is strong and the determination of the rest frequency is less affected by this effect. The same applies to its isotopologues. In the case of Si_2C, most lines show flat profiles (Cernicharo et al. 2015a).

Moderately optically thick lines ($\tau \sim 1$), like those of SiC_2 and the minor isotopologues of SiS and CS, show profiles which are either flat or moderately U-shaped, with a blue peak that can be somewhat weaker than the red one due to self-absorption. The estimated frequency of these lines is in very good agreement with that measured in the laboratory (see top panel of Fig. 2). Around 80% of the lines of these species have δ_ν below 50 kHz, while for the remaining, δ_ν is between 50 and 100 kHz (see Fig. 3).

Extreme examples of very optically thick lines are the rotational transitions of CO, HCN, SiS, CS, and SiO, in which self-absorption in the blue peak is so prominent that central frequencies are systematically shifted towards the red by 0.2–0.5 MHz. Only in these lines the *SHELL* method can provide important systematic effects in the derived central frequency.

An important effect that can modify the shape of the line, and hence, the accuracy of frequency estimates, is pointing errors during the observation. For lines in the 3 mm band this effect is mitigated because the half power width of the main beam is ∼30″ and the source radius for SiC_2, carbon chain radicals, anions, and most species detected with the IRAM 30 m telescope is ∼15″ (Guélin et al. 1993; Velilla Prieto et al. 2015; Agúndez et al. 2017). However, in the 2 mm and 1 mm bands, pointing errors could lead to significant changes in the appearance of the line profile. Depending on the intrinsic shape of the line, the pointing error can produce an increase of the signal around the systemic velocity with a significant decrease at the edges of the line. Hence, the fitted central frequency can be less precise due to the loss of the line horns. In our observations, pointing checks have been performed every hour against a nearby strong continuum source. We can consider that for most lines used in this work the pointing accuracy is better than 2″. Hence, these effects are negligible in the derived frequency uncertainties.

The data shown in Fig. 3 also allow to verify the systemic velocity (v_*) of the source, which was derived by Cernicharo et al. (2000) to be −26.5 km s^{-1} in the Local Standard of Rest (LSR) frame. By assuming that the observed differences δ_ν are due to an incorrect value of v_* we derive a LSR systemic velocity

of -26.51 ± 0.08 km s^{-1} for IRC +10216, in excellent agreement with the value derived by Cernicharo et al. (2000).

4. Frequencies and rotational and centrifugal distortion constants

4.1. SiC_2

Millimetre-wave laboratory spectroscopy of SiC_2 was performed by Gottlieb et al. (1989), who observed 41 rotational lines between 93 and 369 GHz. The dipole moment of the molecule was measured by Suenram et al. (1989), who also reported the frequency of the 1_{01}–0_{00} transition in the centimetre-wave domain for different isotopologues of SiC_2. Using the rotational constants derived by Gottlieb et al. (1989) the frequencies of their reported laboratory lines are obviously well reproduced. However, the energies of the rotational levels becomes negative for $J > 30$. Moreover, frequency predictions for weak transitions of SiC_2 in the 3, 2, and 1 mm domains have large uncertainties. These weak lines are easily detected towards IRC +10216 (see Fig. 1). Better frequency predictions can be obtained by fitting a different set of distortion constants as discussed by Müller et al. (2012). Nevertheless, for frequencies above 400 GHz, frequency predictions for the strongest lines were again very inaccurate by using the laboratory data alone (Cernicharo et al. 2010; Müller et al. 2012).

The observation of IRC +10216 with the HIFI/*Herschel* instrument by Cernicharo et al. (2010) revealed around 300 features between 480 and 1 THz that could be assigned to SiC_2. A detailed analysis of these lines was done by Müller et al. (2012) who provided a global fit to the laboratory and astronomical lines of SiC_2 including those observed with HIFI/*Herschel* and the IRAM 30 m telescope (Cernicharo et al. 2000).

The frequencies of the of SiC_2 transitions between 70 and 350 GHz have been measured again using the new data for IRC +10216. The accuracy of the derived frequencies has improved by a factor of between four and ten for all lines used by Müller et al. (2012). In addition, nearly 100 new rotational lines of SiC_2, many of them corresponding to very weak transitions, have been added to the list of lines observed with the 30 m telescope in this source (see Fig. 1).

Müller et al. (2012) indicated that the accuracy of the frequency determination for the HIFI/*Herschel* lines they used for their global fit was too conservative. Hence, we have analysed again the ~300 rotational transitions observed above 480 GHz and derived new frequencies for these lines. Special care has been taken with possible blends with other species. Although the spectral resolution of these observations was 0.5 MHz, the lines involve high energy levels and show parabolic profiles. Hence, frequency determinations are not as accurate as those obtained from the IRAM 30 m data. For strong features, observed with high signal to noise ratio, the accuracy of the derived frequencies above 480 GHz ranges between 1 and 2 MHz. For lines above 700 GHz we have smoothed the frequency resolution to 2–6 MHz in order to improve the signal to noise ratio of the data. For these, frequency accuracies are between 3 and 6 MHz. Nevertheless, these high-J transitions allow to constraint high order distortion constants in the global fit of the SiC_2 frequencies. Several lines above 900 GHz used in the SiC_2 fit by Müller et al. (2012) have been removed due to poor signal to noise ratio or strong blending with other features.

The list of laboratory and astronomical lines is given in Table A.2. These lines have been fitted using a rotational and distortion Watson Hamiltonian in reduction A representation I^r (Watson 1977) which is described in Appendix A. As commented before (see also Müller et al. 2012) the choice of the parameters to be fitted for the laboratory observations was not the best adapted to the observed range of J and K. In order to compare the different fits that can be obtained for SiC_2 we have explored which distortion constants could be fitted to the laboratory data alone and using the frequency uncertainty for these transitions from Müller et al. (2012). The results are given in Table A.3. The laboratory data alone can be fitted, hence, with a standard deviation of 30 kHz and weighted deviation of 1.1 using up to octic distortion constants. H_J and L_J cannot be accurately derived because the reduced value of J_{max} in the laboratory data set.

Table A.3 also provides the rotational and distortion constants obtained from a fit to the laboratory lines plus those observed with the IRAM 30 m telescope. The improvement in the uncertainty for all rotational and distortion constants varies between a factor 2 and 5. In addition, the distortion constant H_J can be derived from this fit. This combined data set reaches still a rather low J_{max} value of 24, and K_{max} of 12, and it is not possible to derive more octic and some of the decic distortion constants that could be needed to reproduce transitions above the maximum frequency covered in this data set (364.95 GHz). Nevertheless, this set of constants can be used to predict frequencies of the rotational transitions of SiC_2, including those of weak transitions, up to ~500 GHz. The standard deviation of this combined fit is 136 kHz and the weighted standard deviation (*wsd*) is 0.965. This value, close to 1, indicates that the adopted uncertainties for the IRAM data (most of them being ~50 kHz) represents the actual accuracy in the frequency determination of lines with the IRAM 30 m telescope. From this combined set of lines, the standard deviation corresponding only to the laboratory data is again 30 kHz. The degration from 30 to 136 kHz is due to the fact that some lines measured in IRC +10216 above 300 GHz have uncertainties of 0.1–0.3 MHz.

Finally, the HIFI/*Herschel* data have been merged with the laboratory and IRAM data to provide a set of frequencies reaching 1.1 THz, $J_{max} = 53$, and $K_{max} = 16$. Two different sets of distortion constants (A and B in Table A.3) were found to fit reasonably well this merged data set. The main difference between both fits is than in A the distortion constants l_{JK} and P_{JK} are removed and p_{KKJ} is added. Fit B uses the distortion constants of Müller et al. (2012) which provide a standard deviation of 2.2 MHz and a *wsd* of 0.97. We have found that some octic and decic distortion constants were strongly correlated in this fit. Hence, we have explored other sets of distortion constants and found that those given by fit A in Table A.3 are the best adapted to the prediction of frequencies up to 1 THz. With this fit L_J can be derived, together with some decic distortion constants, with very high accuracy. This fit provides a slightly better standard (2.1 MHz) and weighted (0.944) deviations and less correlated distortion constants. With respect to the set of laboratory plus IRAM 30 m lines, the uncertainty on the rotational and the quartic and sextic distortion constants improves by 20–30%. This is the set of molecular parameters that we recommend for the prediction of SiC_2 frequencies below 500 GHz. The HIFI/*Herschel* data help in the determination of the high-order distortion constants but have less effect on the quartic and sextic which are much better constrained by the laboratory and the IRAM data. For frequency predictions above 500 GHz, the parameters derived from the whole set of observed rotational lines, i.e. including the HIFI/*Herschel* data, are recommended. Correlation coefficients between these parameters as derived by fit A are given in Table A.4.

Table 1. Recommended rotational constants for SiC_2, its isotopologues, and Si_2C.

Molecular parameters	Units MHz ×	$^{28}SiC_2^a$	$^{29}SiC_2^b$	$^{30}SiC_2^c$	$^{28}Si^{13}CC^d$	Si_2C^e
A		52474.02946(763)	52472.578(284)	52470.648(307)	50455.638(151)	64074.34272(404)
B		13158.710948(769)	12948.75237(419)	12753.23030(433)	12874.27017(278)	4395.623626(348)
C		10441.580439(714)	10308.81308(486)	10184.40505(493)	10180.85968(261)	4102.024844(630)
Δ_J	10^{-02}	1.317942(334)	1.279225(450)	1.244118(401)	1.270199(417)	0.9732667(877)
Δ_{JK}		1.5383510(443)	1.4972329(685)	1.4592497(621)	1.4571217(823)	−8.571519(556)
Δ_K		−1.267987(478)	−1.2364(239)	−1.2244(237)	−1.2334(158)	23.59437(205)
δ_J	10^{-03}	2.413326(754)	2.31099(374)	2.21188(378)	2.38835(322)	1.524128(254)
δ_K	10^{-01}	8.697376(898)	8.47167(612)	8.25767(607)	8.23435(476)	0.52877(154)
H_J	10^{-07}	−1.4728(794)	−1.4728[f]	−1.4728[f]	−1.4728[f]	−0.35784(513)
H_{JK}	10^{-05}	−4.8821(309)	−4.6357(159)	−4.4451(198)	−3.684(180)	1.9421(109)
H_{KJ}	10^{-04}	3.8901(129)	3.73431(853)	3.6219(118)	3.2920(703)	−18.6228(904)
H_K	10^{-02}	.....	.....	.....	.....	4.9121(180)
h_J	10^{-09}	.....	.....	.....	.....	−4.1625(956)
h_{JK}	10^{-05}	−3.5660(168)	−3.387(120)	−3.419(128)	−3.1254(778)	−0.3441(148)
h_K	10^{-03}	1.07106(575)	1.07106[f]	1.07106[f]	1.0909(385)	.....
L_J	10^{-11}	4.706(558)	4.706[f]	4.706[f]	4.706[f]	.....
L_{JJK}	10^{-09}	−1.211(172)	−1.211[f]	−1.211[f]	−1.211[f]	0.7511(566)
L_{JK}	10^{-07}	−1.3680(208)	−1.3680[f]	−1.3680[f]	−1.3680[f]	−1.2081(781)
L_{KKJ}	10^{-07}	2.051(106)	2.051[f]	2.051[f]	2.051[f]	12.36(259)
P_J	10^{-15}	−9.52(119)	−9.52[f]	−9.52[f]	−9.52[f]	.....
P_{KJ}	10^{-10}	1.3096(919)	1.3096[f]	1.3096[f]	1.3096[f]	.....
P_{KKJ}	10^{-10}	−2.777(462)	−2.777[f]	−2.777[f]	−2.777[f]	.....
p_{KKJ}	10^{-10}	5.894(167)	5.894[f]	5.894[f]	5.894[f]	.....
J_{max}	....	53	16	17	19	45
K_{max}	....	16	8	8	10	5
ν_{max}		1112643.6	359527.359	359324.483	404227.741	350484.8
σ		2.105	0.137	0.123	0.107	0.343
σ_w	....	0.944	1.079	0.976	0.880	0.996

Notes. Numbers in parentheses represent the derived uncertainty (1σ) of the parameter in units of the last digit. [a]From Table A.3. [b]From Table A.6. [c]From Table A.9. [d]From Table A.12. [e]From Table A.15. [f]Fixed to the value derived for the main isotopologue ($^{28}SiC_2$).

Table 2. Determinable Watson's rotational constants, inertia moments, and inertial defect for SiC_2, its isotopologues, and Si_2C.

Constant	Units	$^{28}SiC_2$	$^{29}SiC_2$	$^{30}SiC_2$	$^{28}Si^{13}CC$	Si_2C
A_0	MHz	52474.05582(763)	52472.603(284)	52470.673(307)	50455.664(151)	64074.36218(404)
B_0	MHz	13158.53135(100)	12948.57623(550)	12753.05847(562)	12874.10105(383)	4394.677135(715)
C_0	MHz	10444.889451(946)	10312.03486(617)	10187.54514(623)	10183.99385(366)	4101.295962(997)
I_a	amu Å^2	9.63102727(140)	9.6312937(522)	9.6316481(564)	10.0162998(301)	7.88738344(498)
I_b	amu Å^2	38.40695054(292)	39.0297013(165)	39.6280675(174)	39.2554836(117)	114.9979958(187)
I_c	amu Å^2	48.38529555(438)	49.0086651(293)	49.6075409(303)	49.6248397(178)	123.2242363(299)
Δ	amu Å^2	0.34731772(871)	0.3476700(982)	0.347825(104)	0.3530562(597)	0.3388570(491)

Notes. Numbers in parentheses represent the derived uncertainty (1σ) of the parameter in units of the last digit. I_a, I_b, I_c are the principal inertia moments of the molecule. Δ is the inertial defect ($\Delta = I_b - I_c - I_a$).

The recommended rotational and centrifugal distortion constants for SiC_2 (fit A) are given in Table 1. Watson determinable rotational constants, inertia moments, and the inertial defect are given in Table 2. The molecular parameters resulting from the recommended fit allow to predict well the spectrum of SiC_2 up to 1 THz with uncertainties of a few kHz for the strongest lines, and below 1 MHz for weak lines involving high energy levels.

4.2. $^{29}SiC_2$ and $^{30}SiC_2$

The isotopologues $^{29}SiC_2$ and $^{30}SiC_2$ were identified in IRC +10216 by Cernicharo et al. (1986a). The frequencies of their strongest transitions in the 3 mm domain were calculated using very simple arguments concerning the change of the rotational constants when substituting the silicon atom which lies on the symmetry axis of the molecule. Three lines were

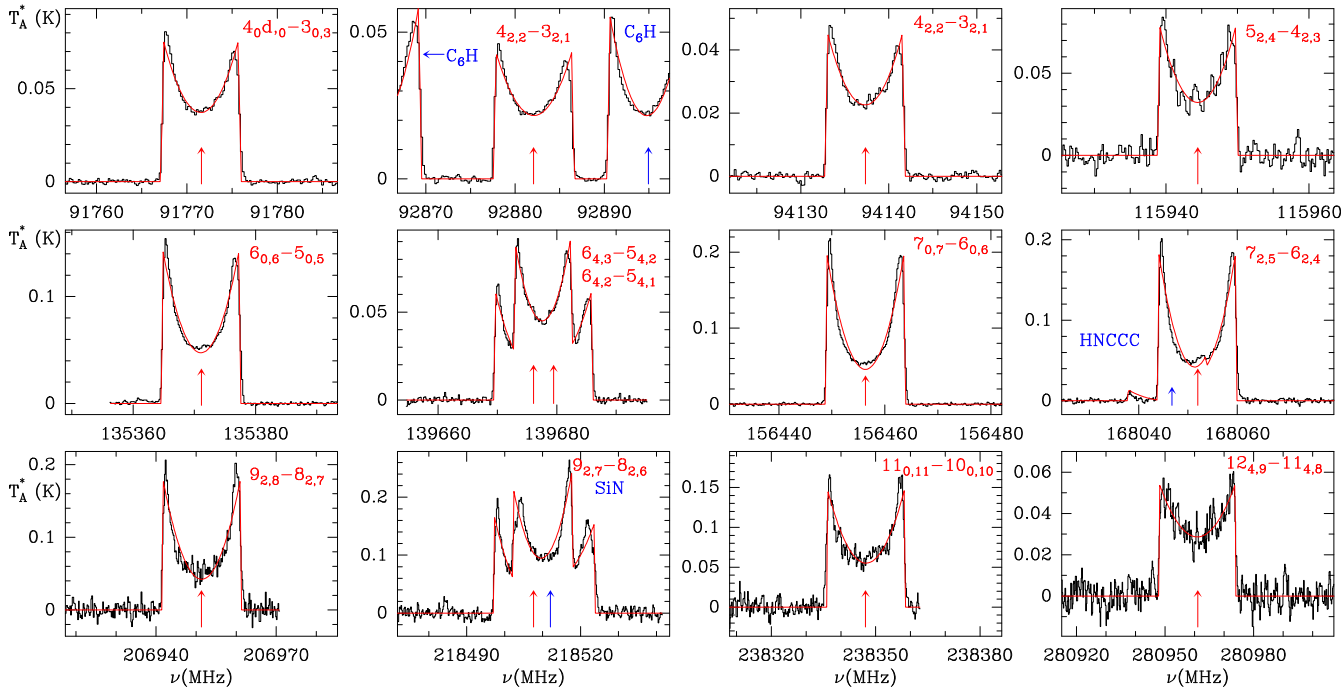

Fig. 4. Selected lines of $^{29}SiC_2$ observed with the new FTS spectrometers installed in the IRAM 30 m telescope after 2010. Red lines show the fit to the observed rotational transitions. The quantum numbers of each transition are indicated at the top-right corner of each panel. Vertical red arrows indicate the fitted frequencies for these transitions. Features from other species are indicated in blue. The sharp edges of the $^{29}SiC_2$ line profiles allow to derive accurate frequencies for these rotational transitions. Measured and fitted frequencies for this isotopologue of SiC_2 are given in Table A.5.

detected within 1 MHz of the predicted frequencies (Cernicharo et al. 1986a). Additional lines of both species were reported by Cernicharo et al. (1991, 2000). Some lines in the 1 mm window were also reported by He et al. (2008) but with poorer frequency accuracies. Laboratory spectroscopy of the 1_{01}–0_{00} transition of both isotopologues was performed by Suenram et al. (1989), and millimetre and submillimetre observations in the laboratory up to 360 GHz were carried out by Kokkin et al. (2011). All lines observed by Cernicharo et al. (1986a, 1991, 2000) have been observed again with the new spectrometers. In addition, 40 new lines have been detected for $^{29}SiC_2$ and 39 for $^{30}SiC_2$ in the 3, 2, and 1 mm domains. Figures 2 and 4 show selected lines of $^{29}SiC_2$, and Fig. 5 shows some of the observed lines of $^{30}SiC_2$. The laboratory and astronomical frequencies are given in Table A.5 for $^{29}SiC_2$ and in Table A.8 for $^{30}SiC_2$.

The J and K coverage is much more modest for these isotopologues than for SiC_2. Hence, it has not been possible to obtain reliable values for the octic and decic centrifugal distortion constants. In the final fit these parameters were fixed to those of the main isotopologue. The derived rotational and centrifugal distortion constants from laboratory data alone and from the combined laboratory + astronomical data fits are given in Tables A.6 and A.9 respectively. A few of the fixed parameters can be derived from the fit with 3–5σ accuracy. However, the derived values are compatible with those of the main isotopologue within the uncertainties. Hence, it is preferable to adopt those of the main isotopologue, which represent the most important contribution to the centrifugal distortion on the frequencies of the rotational transitions of these isotopologues.

The recommended rotational and centrifugal distortion constants for $^{29}SiC_2$ and $^{30}SiC_2$ are given in Table 1. Watson determinable rotational constants, moments of inertia, and the inertial defect are given in Table 2. From the moments of inertia of $^{28}SiC_2$, $^{29}SiC_2$, and $^{30}SiC_2$ it is possible to derive the structural parameters of the molecule, i.e. the SiCC angle (θ), and SiC distance (d_{SiC}), to be $\theta = 40.35(5)^\circ$ and $d_{SiC} = 1.837(1)$ Å. We have adopted the typical uncertainties of bondlengths and angles derived from experimental ground state constants that have been corrected for vibrational effects, which are not studied in this work.

4.3. $Si^{13}CC$

$Si^{13}CC$ was marginally detected by Cernicharo et al. (1986a) in the same work where the silicon isotopologues of SiC_2 were identified. However, the sensitivity of the observations was not enough to carry out a definitive assignment of the lines of the ^{13}C substituted species. Due to molecular symmetry breaking introduced by this substitution, the number of energy levels, and the number of allowed rotational transitions, increases by practically a factor of 2 (the restriction K_a = even disappears).

With the continuous improvement in sensitivity of IRAM 30 m observations, Cernicharo et al. (1991) were able to detect 19 rotational lines of this species up to 160 GHz. Moreover, thanks to the derived rotational and centrifugal distortion constants, it was possible to measure 48 rotational lines in the laboratory between 339 and 404 GHz (Cernicharo et al. 1991). Some frequency improvements for the astrophysical lines were provided by Cernicharo et al. (2000). Additional astronomical lines, but with a poor frequency accuracy (~1–2 MHz), were reported by He et al. (2008).

All the lines reported by Cernicharo et al. (1991, 2000) in the 3 and 2 mm domains have been measured again in this work using the new IRC +10216 data obtained after 2010. Sixteen new lines have been measured in these frequencies domains. In

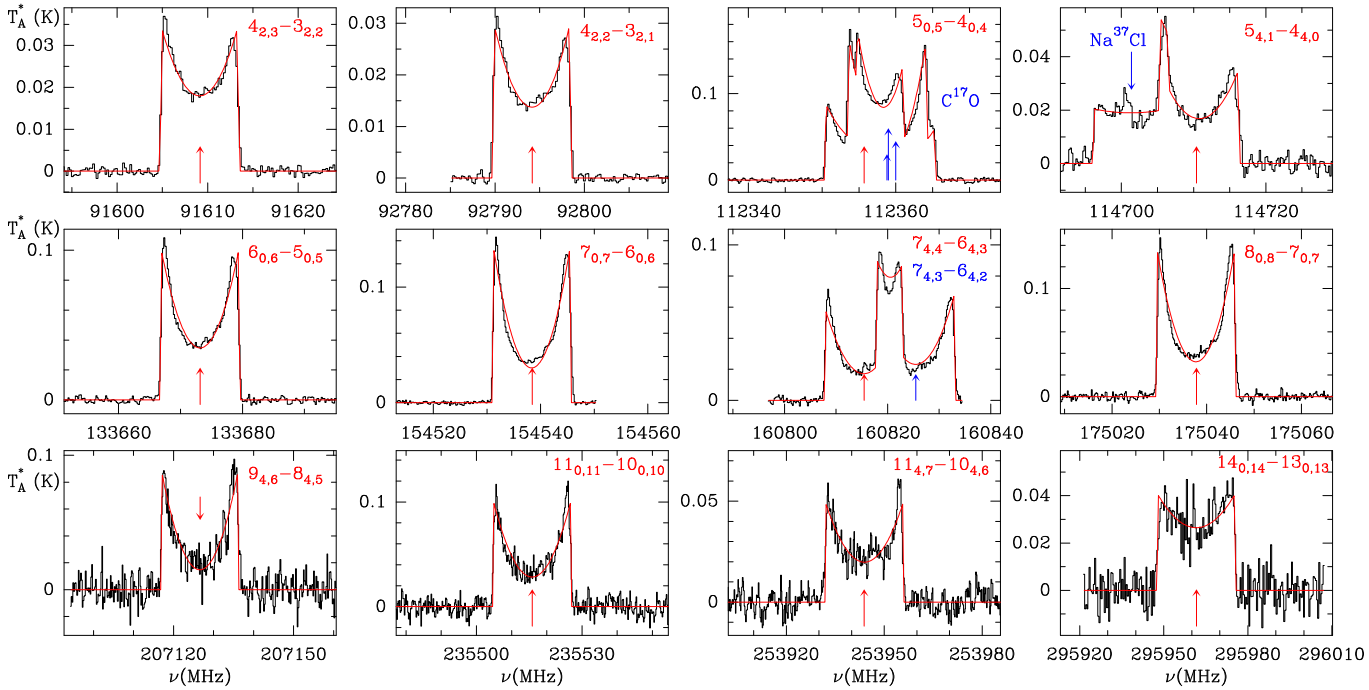

Fig. 5. Same as Fig. 4 but for $^{30}SiC_2$. Measured and fitted frequencies for this isotopologue of SiC_2 are given in Table A.8.

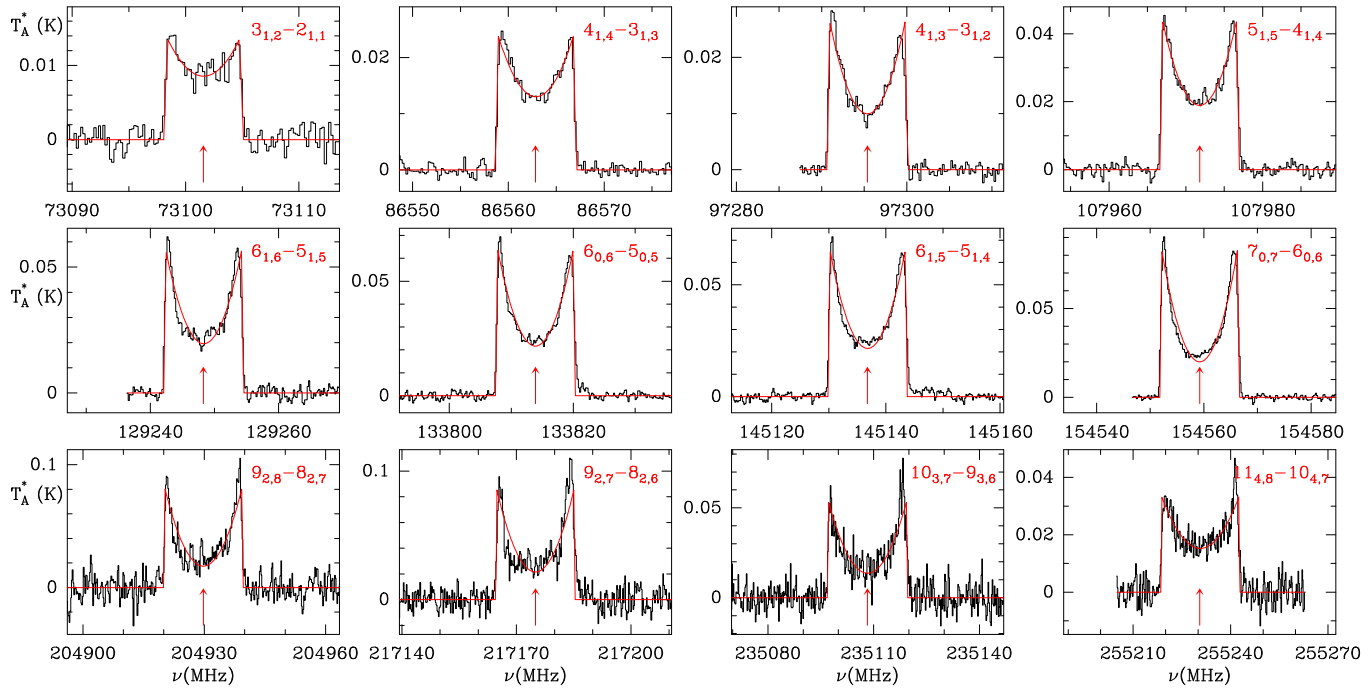

Fig. 6. Same as Fig. 4 but for $Si^{13}CC$. Measured and fitted frequencies for this isotopologue of SiC_2 are given in Table A.11.

addition, 55 lines have been measured in the 1 mm domain, between 197 and 320 GHz. The accuracy of the derived rest frequencies ranges between 50 and 300 kHz for $\nu \leq 295$ GHz, and 0.5 MHz for higher frequencies. Figure 6 shows some of observed lines of $Si^{13}CC$ with 195 kHz spectral resolution. Table A.11 provides the new frequencies for these lines. All frequencies used to fit the molecular parameters of $Si^{13}CC$ are given in Table A.11. The derived rotational and centrifugal distortion constants are given in Table A.12. H_J and the octic and decic centrifugal distortion constants have been fixed to those derived for the main isotopologue. The weighted standard deviation of the fit is 0.88, and the standard deviation is 107 kHz. In this table we provide the molecular parameters derived from a fit to the laboratory data alone, and those obtained from the combined fit to the astronomical and laboratory data. As it could be expected for this isotopologue, for which only high frequency transitions were measured in the laboratory, the improvement of the rotational and centrifugal distortion constants obtained from the combined fit is substantial. The error on the rotational constant A, ΔA, improves by a factor of 2 while for B and C, ΔB and

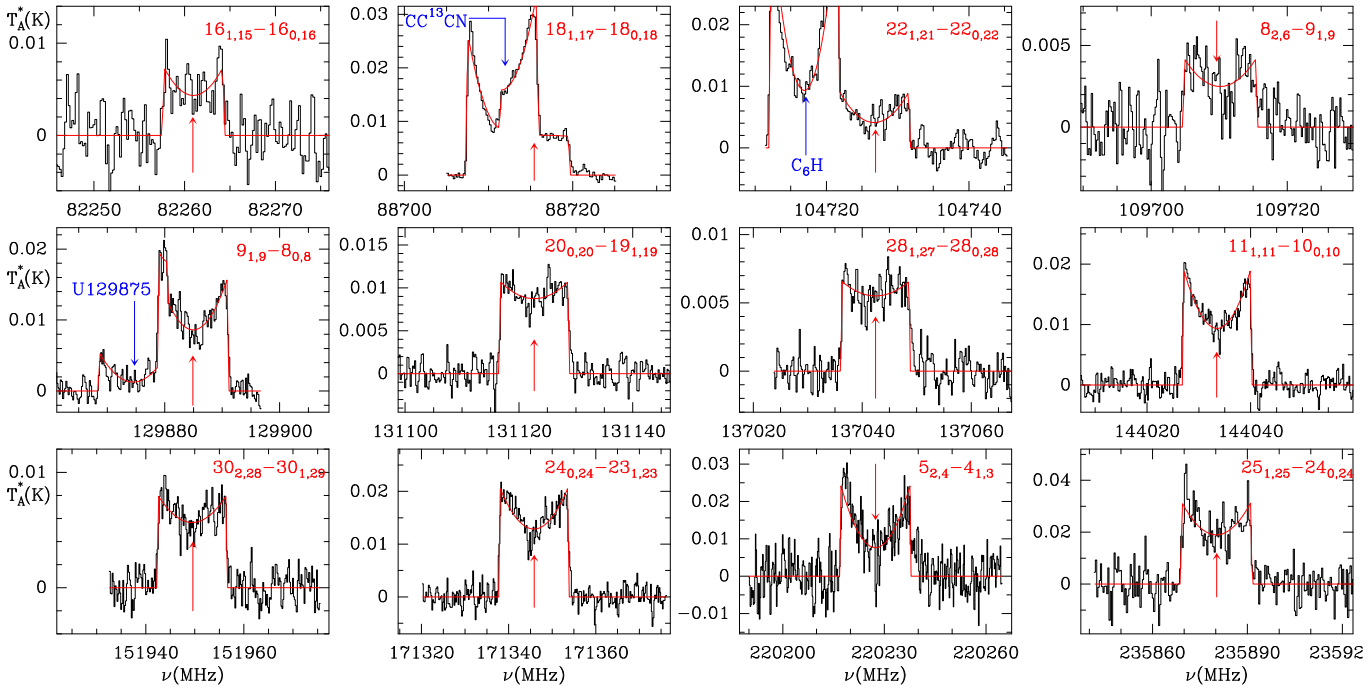

Fig. 7. Same as Fig. 4 but for Si_2C. Measured and fitted frequencies for this species are given in Table A.14.

ΔC, it improves by a factor ~5. The accuracy of the centrifugal distortion constants improves by a factor 2–4.

The molecular parameters resulting from the combined fit allow to predict reasonably well the spectrum of $Si^{13}CC$ up to 400 GHz with uncertainties of a few kHz and for the strongest lines up to 800 GHz with an uncertainty below 1 MHz. These lines correspond to upper energy levels below 600 K.

The recommended rotational and centrifugal distortion constants for $Si^{13}CC$ are given in Table 1. Watson determinable rotational constants, inertia moments, and the inertial defect are given in Table 2.

4.4. Si_2C

Disilicon carbide (SiCSi) was predicted more than 25 yr ago to be an abundant species in the innermost regions of carbon stars based on thermochemical equilibrium calculations (Tsuji 1973; Tejero & Cernicharo 1991; Takano et al. 1992). Several ab initio calculations have been performed on the structure of the molecule (Barone et al. 1992; Bolton et al. 1992; Gabriel et al. 1992; Spielfiedel et al. 1996; McCarthy et al. 2015). However, its search in space was limited by the low brightness temperature expected for its rotational lines, which, when merged with the high line density exhibited by IRC +10216, makes extremely difficult their assignment. Moreover, the limited accuracy obtained by ab initio calculations for the predicted rotational and centrifugal distortion constants implies very poor frequency predictions.

Disilicon carbide has a C_{2v} symmetry and a $^1A_1$ electronic ground state with a modest permanent dipole moment of ~1 D along the *b* axis (McCarthy et al. 2015). Because the two equivalent off-axis silicon atoms are bosons, only half of the rotational levels exist (those with $K_a + K_c$ even). A few lines of this molecule were detected in the laboratory (McCarthy et al. 2015) leading to the identification of 112 lines in IRC +10216 by Cernicharo et al. (2015a) using data taken with the IRAM 30 m telescope prior to 2014. The frequencies of these lines were derived with a spectral resolution of 1 MHz below 270 GHz and of 2 MHz above that frequency. Although the accuracy of frequency determinations was not as good as that presented in this work for SiC_2 and its isotopologues, it was possible to derive a set of molecular parameters permitting reasonably frequency predictions up to 400 GHz with an accuracy better than 0.5 MHz.

The search for lines of SiCSi in space began with the microwave laboratory measurements by McCarthy et al. (2015), which allowed us to accurately predict frequencies with $K_a = 0$, 1 in the 3 mm domain. Cernicharo et al. (2015a) were able to identify 3 lines in that wavelength domain that could be fitted simultaneously with the laboratory data. With the new constants these authors were able to assign 112 lines ($J \leq 48$ and $K_a \leq 5$) in the spectrum of IRC +10216. A fit to all these lines resulted in more accurate frequency predictions, and several additional lines were detected at frequencies up to 180 GHz in the laboratory.

With the new set of high spectral resolution data, it is possible to improve the frequency determination for the previously measured rotational lines of Si_2C (Cernicharo et al. 2015a). Although we are dealing with an abundant species in IRC +10216, the intensity of the lines is rather low, typically below the intensity of the strongest $Si^{13}CC$ lines, which have intensities 40 times less than SiC_2 (see Fig. 6). The reason is the large partition function and moderate dipole moment of Si_2C (Cernicharo et al. 2015a). Nevertheless, we have been able to measure all lines of Si_2C previously reported by Cernicharo et al. (2015a), and to detect new ones, using the IRAM 30 m telescope with the new FTS spectrometers in the 70–180 GHz frequency range. At higher frequencies, data have to be smoothed by two or three channels to have a reasonable signal to noise ratio. We have used all available data to derive frequencies for Si_2C transitions up to 350 GHz. Figure 7 shows some lines of Si_2C observed with a spectral resolution of 195 kHz.

Table A.14 contains the laboratory frequencies measured by McCarthy et al. (2015) and Cernicharo et al. (2015a), together with the astronomical frequencies derived here. Only a few lines could be measured with an accuracy of 50 kHz. However, for most of the lines previously reported by Cernicharo et al. (2015a) the frequency determination has been improved considerably. Fifteen of these lines have been rejected due to a poor accuracy in their frequency determination. In most cases the limited accuracy is due to heavy blending, limited signal to noise ratio, or poorly defined line profiles. Nevertheless, the new data provide 30 new features that can be assigned to rotational transitions of Si_2C. Table A.15 gives the rotational and centrifugal distortion constants obtained by fitting the laboratory data alone, those reported by Cernicharo et al. (2015a), and the ones resulting from a global fit to the laboratory data plus the new Si_2C frequency measurements towards IRC +10216 presented in this work. The weighted standard deviation of the global fit is 0.996 and the standard deviation is 343 kHz (to be compared with the values of 0.837 and 697 kHz obtained by Cernicharo et al. 2015a).

The centrifugal distortion constants Δ_K and Δ_{JK} are much larger for Si_2C than for SiC_2, while the other centrifugal distortion constants are of similar magnitude despite the fact that Si_2C is somewhat heavier than SiC_2. The inertial defect of Si_2C, Δ, is as large as that of SiC_2 (see Table 2). It is assumed that for a triatomic molecule the major contribution to the inertial defect is produced by the lowest frequency vibration of the molecule, $\Delta(\mathrm{amu\,\AA^2}) \sim 67.45/\omega$, where ω is the vibrational frequency in $\mathrm{cm^{-1}}$ (Gordy & Cook 1984). From Table 2 the lowest vibrational frequency of Si_2C is estimated to be $\sim$202 $\mathrm{cm^{-1}}$. This value is somewhat larger than the computed value of 140–150 $\mathrm{cm^{-1}}$ (Spielfiedel et al. 1996; Koput 2017), or the derived value from optical spectroscopy, $\sim$143 $\mathrm{cm^{-1}}$ (Reilly et al. 2015).

It is tempting to search for the isotopologues of Si_2C by using the rotational constants derived from the microwave lines measured by McCarthy et al. (2015), and the centrifugal distortion constants of the main isotopologue derived in this work. Unfortunately, the expected line intensities for ^{29}SiCSi are a factor 20 lower than those of the main isotopologue We note that although there are two identical positions for the ^{29}Si isotope, the partition function increases by a factor of two due to the breaking of the symmetry of the parent molecule. Hence, intensities are directly those of the main isotopologue divided by the isotopic abundance ratio ^{28}Si/^{29}Si $\sim$ 20 (Cernicharo et al. 1986a). A search has been made for the strongest predicted lines of ^{29}SiCSi without success.

The recommended rotational and centrifugal distortion constants for Si_2C are given in Table 1.

5. Conclusions

The frequency accuracy that can be achieved in the millimetre and submillimetre domain with the IRAM 30 m telescope towards IRC +10216 ($\sim$50 kHz) is similar to that obtained in the laboratory ($\sim$30 kHz). Hence, line surveys of IRC +10216 with the 30 m telescope provide, in addition to a determination of molecular abundances, a powerful spectroscopic tool to improve the rotational constants of molecules detected in this source. Hence, thanks to its molecular richness and the range of temperatures exhibited by its circumstellar envelope, IRC +10216 becomes an excellent spectroscopic laboratory for radicals, metal-bearing species, and vibrationally excited states of these species (Cernicharo et al. 2013).

The rotational and centrifugal distortion constants of SiC_2, $^{29}SiC_2$, $^{30}SiC_2$, $Si^{13}CC$, and Si_2C derived in this work can be used to predict accurate frequencies for these species in the ALMA bands, and will help in cleaning the spectrum of IRC +10216 and to identify the hundreds of unidentified lines found in this object (Cernicharo et al. 2013). Moreover, the spectrum of IRC +10216 shows rotational transitions from species such as C_3H, C_4H, C_5H, C_6H, C_7H, and C_8H (Cernicharo et al. 1986b,c, 1987a,b; Guélin et al. 1987), their anions C_4H^-, C_6H^-, C_8H^- (McCarthy et al. 2006; Cernicharo et al. 2007), together with C_3N^- and C_5N^- (Thaddeus et al. 2008; Cernicharo et al. 2008), and of CCS and CCCS (Saito et al. 1987; Yamamoto et al. 1987; Cernicharo et al. 1987c), that are also detected in cold dark molecular clouds. Hence, a systematic analysis of the spectrum of IRC +10216 accessible from the IRAM 30 m telescope will provide, in addition to the discovery of new molecules (some of them being radicals difficult to be produced in the laboratory), an accurate determination of the frequencies of the rotational transitions of species that could be also observed towards other sources.

Acknowledgements. We thank Spanish MINECO for funding support through grants AYA2012-32032 and AYA2016-75066-C2-1-P, and the CONSOLIDER program "ASTROMOL" CSD2009-00038. We thank the European Research Council for funding support under Synergy Grant ERC-2013-SyG, G.A. 610256 (NANOCOSMOS). The data presented in this work have been gathered over a long period of time. We thank the IRAM staff of the 30 m radio telescope for his continuous support during the observations presented in this work. We thank our referee, Carl Gottlieb, for useful comments and suggestions.

References

Agúndez, M., Cernicharo, J., Quintana-Lacaci, G., et al. 2015, ApJ, 814, 143
Agúndez, M., Cernicharo, J., Quintana-Lacaci, G., et al. 2017, A&A, 601, A4
Apponi, A. J., McCarthy, M. C., Gottlieb, C. A., & Thaddeus, P. 1999, ApJ, 516, L103
Barone, V., Jensen, P., & Minichino, C. 1992, J. Mol. Spectr., 154, 252
Bolton, E. E., DeLeeuw, B. J., Fowler, J. E., et al. 1992, J. Chem. Phys., 97, 5586
Bondybey, V. E. 1982, J. Chem. Phys., 86, 3396
Bredohl, H., Dubois, I., Leclercq, H., & Melen, F. 1988, J. Mol. Spectr., 128, 399
Cernicharo, J. 1985, Internal IRAM Report (Granada: IRAM)
Cernicharo, J. 2012, EAS Pub. Ser., 58, 251
Cernicharo, J., & Guélin, M. 1987, A&A, 183, L10
Cernicharo, J., & Guélin, M. 1996, A&A, 309, l27
Cernicharo, J., Kahane, C., Gómez-Gónzalez, J., & Guélin, M. 1986a, A&A, 167, L9
Cernicharo, J., Kahane, C., Gómez-Gónzalez, J., & Guélin, M. 1986b, A&A, 164, L1
Cernicharo, J., Kahane, C., Gómez-Gónzalez, J., & Guélin, M. 1986c, A&A, 167, L5
Cernicharo, J., Guélin, M., Menten, K., & Walmsley, C. M. 1987a, A&A, 181, L1
Cernicharo, J., Walmsley, C. M., & Guélin, M. 1987b, A&A, 172, L5
Cernicharo, J., Kahane, C., Guélin, M., & Hein, H. 1987c, A&A, 181, L9
Cernicharo, J., Gottlieb, C. A., Guélin, et al. 1989 ApJ, 341, L25
Cernicharo, J., Guélin, M., Kahane, C., et al. 1991, A&A, 246, 213
Cernicharo, J., Guélin, M., & Kahane, C. 2000, A&AS, 142, 181
Cernicharo, J., Guélin, M., Agúndez, M., et al. 2007, ApJ, 467, L37
Cernicharo, J., Guélin, M., Agúndez, M., et al. 2008, ApJ, 688, L83
Cernicharo, J., Waters, L. B. F. M., Decin, L., et al. 2010, A&A, 521, L8
Cernicharo, J., Daniel, F., Castro-Carrizo, A., et al. 2013, ApJ, 778, L25
Cernicharo, J., Teyssier, D., Quintana-Lacaci, G., et al. 2014, ApJ, 796, L21
Cernicharo, J., McCarthy, M. C., Gottlieb, C. A., et al. 2015a, ApJ, 806, L3
Cernicharo, J., Marcelino, N., Agúndez, M., & Guélin, M. 2015b, A&A, 575, A91
Cernicharo, J., Agúndez, M., Velilla Prieto, J., et al. 2017, A&A, 606, L5
Chan, S. J., & Kwok, S. 1990, A&A, 237, 354
de Graauw, Th., Helmich, F. P., Phillips, T. G., et al. 2010, A&A, 518, L6
Fortenberry, R. C., Lee, T. J., & Müller, H. S. P. 2015, Mol. Astrophys., 1, 13
Gabriel, W., Chambaud, G., Rosmus, P., et al. 1992, ApJ, 398, 706
Gordy, W., & Cook, R. L. 1984, Microwave Molecular Spectra (New York: Wiley)
Gottlieb, C., Vrtílek, J. M., & Thaddeus, P. 1989, ApJ, 343, L29

Grev, R. S., & Schaefer III, H. F. 1984, J. Chem. Phys., 80, 3552
Guélin, M., Cernicharo, J., Kahane, C., et al. 1987, A&A, 175, L5
Guélin, M., Lucas, R., & Cernicharo, J. 1993, A&A, 280, L19
Guélin, M., Cernicharo, J., Travers, M. J., et al. 1997, A&A, 317, L1
Hackwell, J. A. 1972, A&A, 21, 239
He, J. H., Dinh-V-Trung, Kwok, S., et al. 2008, ApJS, 177, 275
Kisiel, Z. 1990, J. Mol. Spectr., 144, 381
Kisiel, Z. 2001, in Spectroscopy from Space, ed. J. Demaison, et al. (Dordrecht: Kluwer Academic Publishers), 91
Kleman, R. 1956, ApJ, 123, 162
Kokkin, D. L., Brünken, S., Young, K. H., et al. 2011, ApJS, 196. 17
Koput, J. 2016, J. Comput. Chem., 37, 2395
Koput, J. 2017, J. Mol. Spectr., 342, 83
Little-Marenin, I. R. 1986, ApJ, 307, L15
Massalkhi, S., Agúndez, M., Cernicharo, J., et al. 2018, A&A, 611, A29
McCarthy, M. C., Gottlieb, C. A., Gupta, H., & Thaddeus, P. 2006, ApJ, 652, L141
McCarthy, M. C., Baraban, J. H., Changala, P. B., et al. 2015, J. Phys. Chem. Lett., 6, 2107
Merill, P. W. 1926, PASP, 38, 175
Michalopoulos, D. L., Geusic, M. E., Landridge-Smith, P. R. R., & Smalley, R. E. 1984, J. Chem. Phys., 80, 3556
Müller, H. S. P., Schlöder, F., Stutzki, J., & Winnewisser, G. 2005, J. Mol. Struct., 742, 215
Müller, H. S. P., Cernicharo, J., Agúndez, M., et al. 2012, J. Mol. Spectr., 271, 50
Ohishi, M., Kaifu, N., Kawaguchi, K., et al. 1989, ApJ, 345, L83
Pardo, J. R., Cernicharo, J., & Serabyn, E. 2001, IEEE Trans. Antennas Propag., 49, 12
Pardo, J. R., Cernicharo, J., Velilla Prieto, L., et al. 2018, A&A, 615, L4
Patel, N. A., Gottlieb, C. A., & Young, K. H. 2013, in The Life Cycle of Dust in the Universe: Observations, Theory, and Laboratory Experiments, 98
Pickett, H. M. 1991, J. Mol. Spectr., 148, 371
Pickett, H. M., Poynter, R. L., Cohen, E. A., et al. 1998, J. Quant. Spectr. Rad. Transf., 60, 883
Pilbratt, G. L., Riedinger, J. R., Passvogel, T., et al. 2010, A&A, 518, L1
Quintana-Lacaci, G., Agúndez, M., Cernicharo, J., et al. 2016, A&A, 592, A51
Reilly, N. J., Changala, P. B., Baraban, J. H., et al. 2015, J. Chem. Phys., 142, 231101
Sanford, R. F. 1926, PASP, 38, 177
Saito, S., Kawaguchi,, K., Yamamoto, S., et al. 1987, ApJ, 317, L115
Sarre, P., Hurst, M. E., & Evans, T. L. 2000, MNRAS, 319, 103
Spielfiedel, A., Carter, S., Feautrier, N., et al. 1996, J. Phys. Chem., 100, 10055
Suenram, R. D., Lovas, F. J., & Matsumura, K. 1989, ApJ, 342, L103
Tejero, J., & Cernicharo, J. 1991, Modelos de Equilibrio Termodinámico Aplicados a Envolturas Circunestelares de Estrellas Evolucionadas (Madrid: IGN)
Takano, S., Saito, S., & Tsuji, T. 1992, PASJ, 44, 469
Tercero, B., Cernicharo, J., Pardo, J. R., & Goicoechea, J. 2010, A&A, 517, A96
Thaddeus, P., Cummings, S. E., & Linke, R. A. 1984, ApJ, 283, L45
Thaddeus, P., Gottlieb, C. A., Gupta, H., et al. 2008, ApJ, 677, 1132
Treffers, R., & Cohen M. 1974, ApJ, 188, 545
Tsuji, T. 1973, A&A, 23, 411
Velilla Prieto, L., Cernicharo, J., Quintana-Lacaci, G. et al. 2015, ApJ, 805, L13
Yamamoto, S., Saito, S., Kawaguchi, K., et al. 1987, ApJ, 317, L119
Watson, J. K. G. 1977, in Vibration Spectra and Structure, ed. J. Durig, (Amsterdam: Elsevier), 6, 1
Yang, X., Chen, P., & He, J. 2004, A&A, 414, 1049

Appendix A: Frequencies and rotational and centrifugal distortion constants of SiC_2, its isotopologues, and Si_2C

The observed lines described in previous sections have been fitted to a Watson Hamiltonian in reduction A representation I^r, which can be written as (Watson 1977):

$$
\begin{aligned}
H &= A\,P_z^2 + B\,P_x^2 + C\,P_y^2 - \Delta_J\,P^4 - \Delta_{JK}\,P^2P_z^2 - \Delta_K\,P_z^4 \\
&- 2\delta_J\,P^2P_- - \delta_K\,(P_z^2P_- + P_-P_z^2) \\
&+ H_J\,P^6 + H_{JK}\,P^4P_z^2 + H_{KJ}\,P^2P_z^4 + H_K\,P_z^6 \\
&+ 2h_J\,P^4P_- + h_{JK}\,P^2(P_z^2P_- + P_-P_z^2) + h_K\,(P_z^4P_- + P_-P_z^4) \\
&+ L_J\,P^8 + L_{JJK}P^6P_z^2 + L_{JK}\,P^4P_z^4 + L_{KKJ}\,P^2P_z^6 + L_K\,P_z^8 \\
&+ l_J\,P^6P_- + l_{JK}\,P^4(P_z^2P_- + P_-P_z^2) + l_{KJ}\,P^2(P_z^4P_- + P_-P_z^4) \\
&+ l_K\,(P_z^6P_- + P_-P_z^6) \\
&+ P_J\,P^{10} + P_{JJK}\,P^8P_z^2 + P_{JK}\,P^6P_z^4 + P_{KJ}\,P^4P_z^6 + P_{KKJ}\,P^2P_z^8 + P_K\,P_z^{10} \\
&+ p_J\,P^8P_z^2 + p_{JJK}\,P^6(P_z^2P_- + P_-P_z^2) + p_{JK}\,P^4(P_z^4P_- + P_-P_z^4) \\
&+ p_{KKJ}\,P^2(P_z^6P_- + P_-P_z^6) + p_K\,(P_z^8P_- + P_-P_z^8) \qquad \text{(A.1)}
\end{aligned}
$$

where $P_- = (P_x^2 - P_y^2)$, A, B, and C are the effective rotational constants, Δ_J, Δ_{JK}, Δ_K, δ_j, and δ_K are the quartic centrifugal distortion constants, and the parameters H's/h's, L's/l's, and P's/p's represent the sextic, octic, and decic centrifugal distortion constants respectively. The high order centrifugal distortion constants, H, h, L, l, P, p, could be needed to reproduce laboratory frequencies within their accuracy if the molecule is light, or if high-J high-K transitions have been observed. The matrix elements for the operators P_-, P^n, P_x^2, P_y^2, and P_z^n in a symmetric rotor basis can be obtained from the Tables 7.2 and 8.10 of Gordy & Cook (1984).

A code has been developed (*FITWAT*) to fit the observed rotational transitions of an asymmetric rotor and to provide as output, in addition to the rotational and centrifugal distortion constants, a file containing the molecular constants and correlation coefficients. This file can be easily implemented into the MADEX code (Cernicharo 2012) which permits frequency predictions, uncertainties, line strengths, energy levels, and Einstein coefficients for a given J_{max} selected by the user. This way, i.e. collecting molecular parameters rather than line lists, MADEX can digest in a few FORTRAN sentences a molecular species. In the public 2012 version of the code the user can select a molecular species among the 3700 molecules implemented at that time (Cernicharo 2012).

Frequency predictions depend on the accuracy of the derived molecular parameters for a given species. Hence, the fitting program used in this work deserves a benchmark and comparison with other fitting codes. The fitting process starts with a set of initial values for the parameters that have to be obtained. The Hamiltonian contains off-diagonal terms (see, e.g. Watson 1977; Gordy & Cook 1984) and a diagonalization is needed to derive the eigenvectors (as combination of the symmetric rotor basis wave functions) and eigenvalues of the rotational energy levels. Once the eigenvectors are known, the asymmetric rotor energy levels can be directly computed from the expression of the Hamiltonian. A linear least squares method is used to minimize the observed minus calculated frequencies leading to a new set of molecular parameters that is used to compute new eigenvectors and eigenvalues. The process is repeated until the variation of the standard deviation of the fit is less than 10^{-9}.

Table A.1. Benchmark between *FITWAT* and *ASFIT* in fitting data for chlorobenzene.

Molecular parameters	Units MHz ×	*FITWAT*[a]	*ASFIT*[b]
A		5672.2931(133)	5672.2932(133)
B		1576.786974(380)	1576.786976(381)
C		1233.674849(278)	1233.674849(278)
Δ_J	10^{-05}	6.02946(184)	6.02946(184)
Δ_{JK}	10^{-04}	2.81972(111)	2.81973(111)
Δ_K	10^{-04}	9.046(309)	9.047(309)
δ_J	10^{-05}	1.44719(104)	1.44720(104)
δ_K	10^{-04}	3.07111(687)	3.07112(688)
N[c]		186	186
J_{max}	.....	105	105
K_{max}	.....	46	46
ν_{max}		261303.45	261303.45
σ		0.067	0.067
σ_w	.....	0.355	0.355

Notes. Numbers in parentheses represent the derived uncertainty (1σ) of the parameter in units of the last digit. [(a)]Rotational and centrifugal distortion constants obtained by *FITWAT* in the fit to the lines of chlorobenzene reported by Kisiel (1990). [(b)]Rotational and centrifugal distortion constants obtained by *ASFIT* in the fit to the lines of chlorobenzene reported by Kisiel (1990). [(c)]Number of fitted lines (each doublet counts as one single line).

Results from *FITWAT* and Pickett's *SPFIT* code (Pickett 1991) were found to be identical for the data set of Si_2C lines used by Cernicharo et al. (2015a). However, it is important to check the results for high-J and high-K values for which the operators of the asymmetric rotor Hamiltonian can reach very large values. In order to perform such an additional comparison we have fitted the lines of chlorobenzene reported by Kisiel (1990) ($J_{max} = 105$; the molecule is used in the PROSPE[4] package as an example) using *FITWAT* and the code *ASFIT*[5] of the *PROSPE* package of rotational programs developed by Kisiel (2001). The results of both fitting programs are shown in Table A.1. The results are identical within the requested precision of the calculations in *FITWAT*, $\sim 10^{-9}$. Hence, *FITWAT* is feeding MADEX with rotational and centrifugal distortion constants accurately derived from a fit to the available data.

The observed lines of SiC_2, $^{29}SiC_2$, $^{30}SiC_2$, $Si^{13}CC$, and Si_2C are given in Tables A.2, A.5, A.8, and A.14 respectively. The molecular parameters and covariance matrix derived from a fit to the measured frequencies using *FITWAT* are given in Tables A.3 and A.4 for SiC_2, Tables A.6 and A.7 for $^{29}SiC_2$, Tables A.9 and A.10 for $^{30}SiC_2$, Tables A.12 and A.13 for $Si^{13}CC$, and Tables A.15 and A.16 for Si_2C.

[4] http://www.ifpan.edu.pl/~kisiel/prospe.htm
[5] http://www.ifpan.edu.pl/~kisiel/asym/asym.htm

Table A.3. Rotational and centrifugal distortion constants of SiC_2.

Molecular parameters	Units MHz ×	Laboratory[a]	Laboratory[a] + IRAM[b]	Lab[a] + IRAM[b] + HIFI[c]	Lab[a] + IRAM[b] + HIFI[d]
A		52474.1898(774)	52474.03145(857)	52474.02946(763)	52474.02349(801)
B		13158.71481(190)	13158.710065(922)	13158.710948(769)	13158.711999(863)
C		10441.57948(267)	10441.58338(116)	10441.580439(714)	10441.580011(746)
Δ_J	10^{-02}	1.321879(473)	1.318969(485)	1.317942(334)	1.318246(410)
Δ_{JK}		1.538141(100)	1.5383075(501)	1.5383510(443)	1.5383769(454)
Δ_K		−1.2219(182)	−1.268137(509)	−1.267987(478)	−1.268456(491)
δ_J	10^{-03}	2.42102(441)	2.40681(177)	2.413326(754)	2.413465(987)
δ_K	10^{-01}	8.70720(391)	8.69554(129)	8.697376(898)	8.69981(113)
H_J	10^{-07}	....	−1.0877(937)	−1.4728(794)	−1.390(103)
H_{JK}	10^{-05}	−5.932(374)	−4.6759(741)	−4.8821(309)	−4.7495(359)
H_{KJ}	10^{-04}	4.222(124)	3.7967(238)	3.8901(129)	3.8476(147)
h_{JK}	10^{-05}	−2.908(140)	−3.7687(489)	−3.5660(168)	−3.5116(375)
h_K	10^{-03}	0.8667(717)	1.1055(141)	1.07106(575)	1.09098(701)
L_J	10^{-11}	....	....	4.706(558)	3.795(713)
L_{JJK}	10^{-09}	−4.68(101)	−4.648(734)	−1.211(172)	−2.555(149)
L_{JK}	10^{-07}	−1.0414(903)	−1.2421(215)	−1.3680(208)	−1.3992(212)
L_{KKJ}	10^{-07}	1.477(250)	2.2275(504)	2.051(106)	2.302(111)
l_{JK}	10^{-09}	....	....	....	−1.010(184)
P_J	10^{-15}	....	....	−9.52(119)	−7.61(139)
P_{JK}	10^{-11}	....	....	....	−3.614(115)
P_{KJ}	10^{-10}	....	....	1.3096(919)	2.777(130)
P_{KKJ}	10^{-10}	....	....	−2.777(462)	−5.147(518)
p_{KKJ}	10^{-10}	....	....	5.894(167)	....
N[e]	....	30	125	579	579
$J_{\max}$	....	17	24	53	53
$K_{\max}$	....	10	12	16	16
$\nu_{\max}$		364948.2	364948.2	1112643.6	1112643.6
σ		0.030	0.136	2.105	2.211
σ_w	....	1.128	0.965	0.944	0.968

Notes. Numbers in parentheses represent the derived uncertainty (1σ) of the parameter in units of the last digit. [(a)]Fit to the rotational lines reported by Gottlieb et al. (1989) and Suenram et al. (1989). Uncertainties for these lines are from Müller et al. (2012). [(b)]New lines between 70 and 355 GHz have been added to the data set reported by Müller et al. (2012). The increase in sensitivity and spectral resolution in the IRAM data since 2012 have permitted to obtain more precise frequencies in that frequency range. Frequencies for all lines used by Müller et al. (2012) have been determined using the new IRAM 30 m data. [(c)]The selected HIFI data are from Cernicharo et al. (2010) and Müller et al. (2012). Frequencies for HIFI lines have been measured again taken into account possible blends with other features. Some of the lines reported by Müller et al. (2012) have been rejected due to its poor signal to noise ratio (see text). This column corresponds to Fit *A* and is the recommended one. [(d)]Fit *B* uses the same set of data as 3 but adding to the fitted centrifugal distortion constants l_{JK} and P_{JK}, and removing p_{KKJ} (see text). [(e)]Number of fitted lines (each doublet counts as one single line).

Table A.4. Correlation coefficients for the recommended rotational and centrifugal distortion constants of SiC_2.

Constant	A	B	C	Δ_J	Δ_{JK}	Δ_K	δ_J	δ_K	H_J	H_{JK}	H_{KJ}	h_{JK}	h_K	L_J	L_{JJK}	L_{JK}	L_{KKJ}	P_J	P_{JK}	P_{KKJ}	p_{KKJ}
A	1.000																				
B	0.035	1.000																			
C	0.352	0.256	1.000																		
Δ_J	0.050	0.670	0.619	1.000																	
Δ_{JK}	0.278	0.559	0.254	0.231	1.000																
Δ_K	0.576	−0.014	0.034	−0.046	0.018	1.000															
δ_J	−0.114	0.475	−0.397	−0.007	0.142	0.033	1.000														
δ_K	−0.316	0.346	−0.337	0.265	0.211	−0.169	0.048	1.000													
H_J	0.004	0.480	0.504	0.940	0.070	−0.060	−0.093	0.255	1.000												
H_{JK}	−0.001	0.297	0.100	0.159	0.402	−0.201	−0.296	0.367	0.079	1.000											
H_{KJ}	0.184	0.247	0.048	0.107	0.547	0.170	0.373	0.047	0.059	−0.489	1.000										
h_{JK}	−0.163	0.329	−0.301	0.185	0.129	−0.082	0.664	0.507	0.154	−0.278	0.438	1.000									
h_K	−0.123	0.197	−0.049	0.089	0.213	−0.242	−0.358	0.482	0.067	0.943	−0.560	−0.291	1.000								
L_J	−0.007	−0.427	−0.450	−0.854	−0.065	0.062	0.132	−0.216	−0.953	−0.151	0.009	−0.063	−0.158	1.000							
L_{JJK}	−0.103	0.149	−0.315	−0.046	0.031	−0.052	0.526	0.268	−0.023	−0.210	0.266	0.729	−0.164	−0.039	1.000						
L_{JK}	−0.091	−0.367	−0.038	−0.187	−0.451	0.075	−0.345	−0.208	−0.104	−0.347	−0.102	−0.495	−0.171	0.138	−0.614	1.000					
L_{KKJ}	−0.078	−0.247	−0.005	−0.105	−0.563	−0.047	0.039	−0.318	−0.073	−0.067	−0.636	−0.001	−0.110	0.052	0.163	−0.233	1.000				
P_J	0.017	0.361	0.421	0.769	0.053	−0.050	−0.167	0.167	0.884	0.154	−0.032	−0.007	0.166	−0.977	0.012	−0.101	−0.051	1.000			
P_{JK}	0.051	0.213	−0.039	0.082	0.233	−0.033	0.400	0.106	0.040	0.006	0.171	0.568	−0.111	−0.063	0.762	−0.866	0.380	0.026	1.000		
P_{KKJ}	0.045	0.109	0.052	0.071	0.318	0.028	−0.225	0.180	0.055	0.189	0.282	−0.278	0.238	−0.037	−0.491	0.441	−0.854	0.051	−0.726	1.000	
p_{KKJ}	−0.075	0.091	−0.266	−0.072	−0.010	−0.022	0.489	0.174	−0.055	−0.307	0.273	0.677	−0.267	0.015	0.952	−0.525	0.224	−0.042	0.792	−0.601	1.000

Table A.6. Rotational and centrifugal distortion constants of $^{29}SiC_2$.

Molecular parameters	Units MHz ×	Laboratory[a]	Laboratory[a] + IRAM[b]	Laboratory[a] + IRAM[c]
A		52472.405(316)	52472.578(284)	52476.503(285)
B		12948.75039(483)	12948.75237(419)	12948.79985(469)
C		10308.82104(596)	10308.81308(486)	10308.76204(493)
Δ_J	10^{-02}	1.279872(536)	1.279225(450)	1.27882(153)
Δ_{JK}		1.4973073(857)	1.4972329(685)	1.4961945(938)
Δ_K		−1.2506(261)	−1.2364(239)	−0.7758(243)
δ_J	10^{-03}	2.30710(466)	2.31099(374)	2.35673(401)
δ_K	10^{-01}	8.46383(750)	8.47167(612)	8.46116(887)
H_J	10^{-07}	−1.4728[e]	−1.4728[e]	−1.392(418)
H_{JK}	10^{-05}	−4.6168(192)	−4.6357(159)	−10.1075(247)
H_{KJ}	10^{-04}	3.73460(922)	3.73431(853)	5.29975(856)
h_{JK}	10^{-05}	−3.555(152)	−3.387(120)	−3.531(217)
h_K	10^{-03}	1.07106[e]	1.07106[e]	....
L_J	10^{-11}	4.706[e]	4.706[e]	....
L_{JJK}	10^{-09}	−1.211[e]	−1.211[e]	....
L_{JK}	10^{-07}	−1.3680[e]	−1.3680[e]	....
L_{KKJ}	10^{-07}	2.051[e]	2.051[e]	....
P_J	10^{-15}	−9.52[e]	−9.52[e]	....
P_{KJ}	10^{-10}	1.3096[e]	1.3096[e]	....
P_{KKJ}	10^{-10}	−2.777[e]	−2.777[e]	....
p_{KKJ}	10^{-10}	5.894[e]	5.894[e]	....
N[d]	....	34	83	83
J_{max}	....	16	16	16
K_{max}	....	8	8	8
ν_{max}		359527.359	359527.359	359527.359
σ		0.034	0.134	0.138
σ_w	....	1.151	1.079	1.076

Notes. Numbers in parentheses represent the derived uncertainty (1σ) of the parameter in units of the last digit. [(a)]Fit to the rotational lines reported by Kokkin et al. (2011) and Suenram et al. (1989). [(b)]Lines observed with the IRAM 30 m telescope between 70 and 320 GHz. Frequencies reported by Cernicharo et al. (1986a, 1991, 2000) have been measured again with the new FTS spectrometers at a spectral resolution of 195 kHz. This is the recommended fit to predict rotational frequencies for $^{29}SiC_2$. [(c)]Same set of frequencies and fitting than 2 but fixing to zero the octic and decic centrifugal distortion constants. [(d)]Number of fitted lines (each doublet counts as one single line). [(e)]These constants have been fixed to the corresponding value for the main isotopologue $^{28}SiC_2$.

Table A.7. Correlation coefficients for the recommended rotational and centrifugal distortion constants of $^{29}SiC_2$.

Constant	A	B	C	Δ_J	Δ_{JK}	Δ_K	δ_J	δ_K	H_{JK}	Δ_{KJ}	h_{JK}
A	1.000										
B	0.845	1.000									
C	–0.803	–0.860	1.000								
Δ_J	–0.387	–0.060	0.400	1.000							
Δ_{JK}	–0.156	–0.027	0.361	0.293	1.000						
Δ_K	0.857	0.775	–0.772	–0.319	–0.139	1.000					
δ_J	0.388	0.703	–0.768	–0.033	–0.249	0.305	1.000				
δ_K	0.405	0.540	–0.747	–0.180	–0.343	0.666	0.584	1.000			
H_{JK}	–0.037	0.071	0.311	0.580	0.649	–0.204	–0.093	–0.472	1.000		
H_{KJ}	–0.350	–0.167	0.189	0.071	0.592	–0.106	–0.118	0.147	–0.123	1.000	
h_{JK}	0.182	0.296	–0.617	–0.360	–0.402	0.316	0.638	0.849	–0.547	0.130	1.000

Table A.9. Rotational and centrifugal distortion constants of $^{30}SiC_2$.

Molecular parameters	Units MHz ×	Laboratory[a]	Laboratory[a] + IRAM[b]	Laboratory[a] + IRAM[c]
A		52470.700(355)	52470.648(307)	52474.610(331)
B		12753.23184(512)	12753.23030(433)	12753.27254(489)
C		10184.40704(616)	10184.40505(493)	10184.35636(535)
Δ_J	10^{-02}	1.244536(504)	1.244118(401)	1.24057(144)
Δ_{JK}		1.4592525(816)	1.4592497(621)	1.4582939(923)
Δ_K		–1.2238(274)	–1.2244(237)	–0.7676(263)
δ_J	10^{-03}	2.21113(486)	2.21188(378)	2.25294(418)
δ_K	10^{-01}	8.25471(817)	8.25767(607)	8.2297(104)
H_J	10^{-07}	–1.4728[e]	–1.4728[e]	–2.168(371)
H_{JK}	10^{-05}	–4.4381(250)	–4.4451(198)	–9.7273(304)
H_{KJ}	10^{-04}	3.6183(139)	3.6219(118)	5.1106(134)
h_{JK}	10^{-05}	–3.503(179)	–3.419(128)	–3.979(246)
h_K	10^{-03}	1.07106[e]	1.07106[e]	....
L_J	10^{-11}	4.706[e]	4.706[e]	....
L_{JJK}	10^{-09}	–1.211[e]	–1.211[e]	....
L_{JK}	10^{-07}	–1.3680[e]	–1.3680[e]	....
L_{KKJ}	10^{-07}	2.051[e]	2.051[e]	....
P_J	10^{-15}	–9.52[e]	–9.52[e]	....
P_{KJ}	10^{-10}	1.3096[e]	1.3096[e]	....
P_{KKJ}	10^{-10}	–2.777[e]	–2.777[e]	....
p_{KKJ}	10^{-10}	5.894[e]	5.894[e]	....
N[d]	....	32	76	76
J_{max}	....	16	17	17
K_{max}	....	8	8	8
ν_{max}		359324.483	359324.483	359324.483
σ(MHz)		0.044	0.123	0.126
σ_w	....	1.102	0.977	1.055

Notes. Numbers in parentheses represent the derived uncertainty (1σ) of the parameter in units of the last digit. [(a)]Fit to the rotational lines reported by Kokkin et al. (2011) and Suenram et al. (1989). [(b)]Lines observed with the IRAM 30 m telescope between 70 and 320 GHz. Frequencies reported by Cernicharo et al. (1986a, 1991, 2000) have been measured again with the new FTS spectrometers at a spectral resolution of 195 kHz.This is the recommended fit to predict rotational frequencies for $^{30}SiC_2$. [(c)]Same set of frequencies and fitting than 2 but fixing to zero the octic and decic centrifugal distortion constants. [(d)]Number of fitted lines (each doublet counts as one single line). [(e)]These constants have been fixed to the corresponding value for the main isotopologue $^{28}SiC_2$.

Table A.10. Correlation coefficients for the rotational and centrifugal distortion constants of $^{30}SiC_2$.

Constant	A	B	C	Δ_J	Δ_{JK}	Δ_K	δ_J	δ_K	H_{JK}	Δ_{KJ}	h_{JK}
A	1.000										
B	0.885	1.000									
C	–0.840	–0.879	1.000								
Δ_J	–0.329	–0.049	0.379	1.000							
Δ_{JK}	–0.165	–0.060	0.374	0.317	1.000						
Δ_K	0.883	0.780	–0.789	–0.397	–0.149	1.000					
δ_J	0.491	0.739	–0.794	0.010	–0.292	0.332	1.000				
δ_K	0.457	0.564	–0.780	–0.292	–0.387	0.631	0.653	1.000			
H_{JK}	0.221	0.287	0.018	0.510	0.468	–0.043	0.174	–0.313	1.000		
H_{KJ}	–0.512	–0.432	0.373	–0.079	0.308	–0.221	–0.405	–0.005	–0.655	1.000	
h_{JK}	0.256	0.369	–0.656	–0.373	–0.431	0.314	0.713	0.881	–0.302	–0.054	1.000

Table A.12. Rotational and centrifugal distortion constants of $Si^{13}CC$.

Molecular parameters	Units MHz ×	Laboratory[a]	Laboratory[a] + IRAM[b]	Laboratory[a] + IRAM[c]
A		50455.863(330)	50455.638(151)	50455.759(194)
B		12874.2710(145)	12874.27017(278)	12874.26839(319)
C		10180.8358(163)	10180.85968(261)	10180.85745(283)
Δ_J	10^{-02}	1.26862(200)	1.270199(417)	1.26780(139)
Δ_{JK}		1.457061(258)	1.4571217(823)	1.456839(186)
Δ_K		–1.2095(221)	–1.2334(158)	–1.2167(255)
δ_J	10^{-03}	2.39947(917)	2.38835(322)	2.39016(359)
δ_K	10^{-01}	8.2526(141)	8.23435(476)	8.22431(864)
H_J	10^{-07}	–1.4728[e]	–1.4728[e]	–1.763(291)
H_{JK}	10^{-05}	–3.824(211)	–3.684(180)	–4.160(385)
H_{KJ}	10^{-04}	3.3429(885)	3.2920(703)	3.361(131)
h_{JK}	10^{-05}	–2.791(261)	–3.1254(778)	–3.331(159)
h_K	10^{-03}	1.0599(489)	1.0909(385)	1.0282(717)
L_J	10^{-11}	4.706[e]	4.706[e]	....
L_{JJK}	10^{-09}	–1.211[e]	–1.211[e]	....
L_{JK}	10^{-07}	–1.3680[e]	–1.3680[e]	–1.302(109)
L_{KKJ}	10^{-07}	2.051[e]	2.051[e]	2.557(383)
P_J	10^{-15}	–9.52[e]	–9.52[e]	....
P_{KJ}	10^{-10}	1.3096[e]	1.3096[e]	....
P_{KKJ}	10^{-10}	–2.777[e]	–2.777[e]	....
p_{KKJ}	10^{-10}	5.894[e]	5.894[e]	....
N[d]	....	48	129	129
J_{max}	....	19	19	19
K_{max}	....	10	10	10
ν_{max}		404227.741	404227.741	404227.741
σ		0.068	0.107	0.111
σ_w	....	0.668	0.880	0.889

Notes. Numbers in parentheses represent the derived uncertainty (1σ) of the parameter in units of the last digit. [(a)]Fit to the rotational lines reported by Cernicharo et al. (1991). [(b)]Lines observed with the IRAM 30 m telescope between 70 and 320 GHz. Frequencies reported by Cernicharo et al. (1991, 2000) have been measured again with the new FTS spectrometers at a spectral resolution of 195 kHz.This is the recommended fit to predict rotational frequencies for $Si^{13}CC$. [(c)]Same set of frequencies and fitting than 2 but fixing to zero some of the octic and decic centrifugal distortion constants. [(d)]Number of fitted lines (each doublet counts as one single line). [(e)]These constants have been fixed to the corresponding value for the main isotopologue $^{28}SiC_2$.

Table A.13. Correlation coefficients for the rotational and centrifugal distortion constants of $Si^{13}CC$.

Constant	A	B	C	Δ_J	Δ_{JK}	Δ_K	δ_J	δ_K	H_{JK}	Δ_{KJ}	h_{JK}	h_K
A	1.000											
B	0.618	1.000										
C	–0.430	–0.639	1.000									
Δ_J	0.001	0.498	–0.002	1.000								
Δ_{JK}	0.352	0.453	0.085	0.291	1.000							
Δ_K	0.790	0.577	–0.474	0.244	0.292	1.000						
δ_J	0.318	0.743	–0.673	0.466	0.253	0.392	1.000					
δ_K	–0.238	0.059	–0.551	0.040	–0.377	0.127	0.174	1.000				
H_{JK}	–0.635	–0.505	0.263	–0.347	–0.441	–0.730	–0.616	0.285	1.000			
H_{KJ}	0.625	0.525	–0.247	0.371	0.516	0.725	0.614	–0.290	–0.995	1.000		
h_{JK}	–0.213	–0.002	–0.573	–0.228	–0.337	–0.035	0.345	0.813	0.159	–0.177	1.000	
h_K	–0.638	–0.526	0.246	–0.381	–0.489	–0.722	–0.625	0.308	0.997	–0.996	0.184	1.000

Table A.15. Rotational and centrifugal distortion constants of Si_2C.

Molecular parameters	Units MHz ×	Laboratory[a]	Laboratory[a] + IRAM[b]	Laboratory[a] + IRAM[c]
A		64074.13878(378)	64074.33635(369)	64074.34272(404)
B		4395.62952(799)	4395.621073(843)	4395.623626(348)
C		4102.01836(783)	4102.02790(107)	4102.024844(630)
Δ_J	10^{-03}	9.74594(630)	9.73137(179)	9.732667(877)
Δ_{JK}	10^{-01}	–8.56821(162)	–8.572108(612)	–8.571519(556)
Δ_K		23.34171(174)	23.58814(148)	23.59437(205)
δ_J	10^{-03}	1.52762(206)	1.519825(437)	1.524128(254)
δ_K	10^{-02}	5.592(390)	5.1592(453)	5.2877(154)
H_J	10^{-08}	....	–4.1410(948)	–3.5784(513)
H_{JK}	10^{-05}	2.2343(984)	1.93254(547)	1.9421(109)
H_{KJ}	10^{-03}	–1.9365(312)	–1.88712(796)	–1.86228(904)
H_K	10^{-02}	....	4.8622(170)	4.9121(180)
h_J	10^{-09}	....	–5.233(186)	–4.1625(956)
h_{JK}	10^{-06}	....	–6.586(361)	–3.441(148)
L_{JJK}	10^{-10}	....	....	7.511(566)
L_{JK}	10^{-07}	....	....	–1.2081(781)
L_{KKJ}	10^{-06}	....	....	1.236(259)
N[d]	....	22	134	149
J_{max}	....	20	48	45
K_{max}	....	2	5	5
ν_{max}		185976.78	350484.8	350484.8
σ		0.022	0.697	0.343
σ_w	....	0.684	0.837	0.996

Notes. Numbers in parentheses represent the derived uncertainty (1σ) of the parameter in units of the last digit. [(a)]Fit to the laboratory lines reported by Cernicharo et al. (2015a) (see also McCarthy et al. 2015). [(b)]Rotational constants from Cernicharo et al. (2015a) derived from a fit to the laboratory and 30 m lines. [(c)]Rotational constants derived from the laboratory frequencies, the revised frequency for the lines observed with the IRAM 30 m telescope from Cernicharo et al. (2015a), and those of the new observed lines with the same telescope (see text). [(d)]Number of fitted lines.

Table A.16. Correlation coefficients for the rotational and centrifugal distortion constants of Si_2C.

Constant	A	B	C	Δ_J	Δ_{JK}	Δ_K	δ_J	δ_K	H_J	H_{JK}	H_{KJ}	H_K	h_J	h_{JK}	L_{JJK}	L_{JK}	L_{KKJ}
A	1.000																
B	0.570	1.000															
C	0.675	0.046	1.000														
Δ_J	0.522	0.224	0.640	1.000													
Δ_{JK}	–0.198	–0.312	0.112	0.240	1.000												
Δ_K	0.766	0.433	0.332	0.178	–0.536	1.000											
δ_J	–0.275	0.346	–0.798	–0.417	–0.378	–0.003	1.000										
δ_K	–0.232	0.571	–0.706	–0.408	–0.051	–0.099	0.703	1.000									
H_J	0.328	0.293	0.288	0.823	0.207	0.114	–0.106	–0.094	1.000								
H_{JK}	–0.454	–0.362	–0.021	–0.001	0.797	–0.784	–0.329	0.020	0.032	1.000							
H_{KJ}	0.324	–0.048	0.113	0.130	0.325	0.418	–0.146	–0.086	0.125	–0.238	1.000						
H_K	0.450	0.337	0.224	0.084	–0.529	0.645	0.038	–0.039	0.015	–0.412	–0.236	1.000					
h_J	–0.268	0.074	–0.603	–0.388	–0.383	–0.024	0.858	0.340	–0.170	–0.316	–0.216	0.086	1.000				
h_{JK}	–0.085	0.630	–0.621	–0.283	–0.174	0.083	0.813	0.907	–0.014	–0.216	0.004	0.043	0.484	1.000			
L_{JJK}	0.396	0.431	–0.084	0.095	–0.453	0.643	0.361	0.185	0.148	–0.791	0.482	0.128	0.181	0.379	1.000		
L_{JK}	–0.032	–0.024	0.120	–0.077	–0.442	–0.017	0.006	–0.189	–0.198	–0.093	–0.696	0.486	0.240	–0.165	–0.482	1.000	
L_{KKJ}	–0.438	–0.069	–0.287	–0.076	0.271	–0.636	0.122	0.234	0.059	0.403	–0.174	–0.757	–0.026	0.119	–0.026	–0.460	1.000